

ARTICLE

Myeloid activation clears ascites and reveals IL27-dependent regression of metastatic ovarian cancer

Brennah Murphy^{1*}, Taito Miyamoto^{1,3*}, Bryan S. Manning^{1,7}, Gauri Mirji¹, Alessio Ugolini¹, Toshitha Kannan², Kohei Hamada³, Yanfang P. Zhu⁴, Daniel T. Claiborne¹, Lu Huang⁵, Rugang Zhang^{1,6}, Yulia Nefedova¹, Andrew Kossenkov², Filippo Veglia¹, Rahul Shinde¹, and Nan Zhang¹

Patients with metastatic ovarian cancer (OvCa) have a 5-year survival rate of <30% due to the persisting dissemination of chemoresistant cells in the peritoneal fluid and the immunosuppressive microenvironment in the peritoneal cavity. Here, we report that intraperitoneal administration of β -glucan and IFN γ (BI) induced robust tumor regression in clinically relevant models of metastatic OvCa. BI induced tumor regression by controlling fluid tumor burden and activating localized antitumor immunity. β -glucan alone cleared ascites and eliminated fluid tumor cells by inducing intraperitoneal clotting in the fluid and Dectin-1-Syk-dependent NETosis in the omentum. In omentum tumors, BI expanded a novel subset of immunostimulatory IL27⁺ macrophages and neutralizing IL27 impaired BI efficacy *in vivo*. Moreover, BI directly induced IL27 secretion in macrophages where single agent treatment did not. Finally, BI extended mouse survival in a chemoresistant model and significantly improved chemotherapy response in a chemo-sensitive model. In summary, we propose a new therapeutic strategy for the treatment of metastatic OvCa.

Introduction

Ovarian cancer (OvCa) is the most lethal gynecological cancer in the United States and the fifth leading cause of cancer-related deaths in women due in large part to metastases (Siegel et al., 2023). Unlike other cancers that metastasize through circulation, OvCa cells mostly disseminate directly into the peritoneal cavity and preferentially seed in the omentum prior to metastasizing to other peritoneal organs (Ma, 2020). Because it is difficult to detect at early stages, OvCa is often diagnosed at later stages with metastatic lesions present throughout the peritoneal cavity (stages III and IV) (Lengyel, 2010). Despite an initial positive response to chemotherapy, most patients relapse and ultimately present with intraperitoneal chemoresistant disease and poor prognosis (Colombo et al., 2017). Meanwhile, recent breakthroughs in immune checkpoint therapies have led to little improvement in OvCa prognosis (Monk et al., 2021; Pujade-Lauraine et al., 2021). Therefore, there is an urgent need to develop alternative therapies for end-stage metastatic OvCa.

Multiple mechanisms contribute to therapy resistance in metastatic OvCa. First, the presence of disseminated cancer cells in the peritoneal fluid following initial treatment may promote therapy resistance in relapsed patients (Shield et al., 2009). A growing body of evidence suggests that these disseminating cells, which are present in malignant ascites and cannot be surgically resected, exhibit cancer stem cell characteristics that render them highly invasive and broadly resistant to therapy (Latifi et al., 2012; Liao et al., 2014; Shepherd and Dick, 2022; Shield et al., 2009; Ward Rashidi et al., 2019). Targeting these cells remains a significant challenge to overcoming therapy resistance and relapse.

The second mechanism of therapy resistance is likely driven by the highly immunosuppressive microenvironment in the peritoneal cavity (Almeida-Nunes et al., 2022). Its immunosuppressive nature is predominantly supported by myeloid cells, namely macrophages (M Φ s) and neutrophils, which are the

¹Immunology, Microenvironment and Metastasis Program, Ellen and Ronald Caplan Cancer Center, The Wistar Institute, Philadelphia, PA, USA; ²Gene Expression and Regulation Program, Ellen and Ronald Caplan Cancer Center, The Wistar Institute, Philadelphia, PA, USA; ³Department of Gynecology and Obstetrics, Kyoto University Graduate School of Medicine, Kyoto, Japan; ⁴Medical College of Georgia, Augusta University, Augusta, GA, USA; ⁵Department of Microbiology and Immunology, University of Arkansas for Medical Sciences, Little Rock, AR, USA; ⁶Department of Experimental Therapeutics, MD Anderson Cancer Center, Houston, TX, USA; ⁷Cancer Biology Graduate Program, Saint Joseph's University, Philadelphia, PA, USA.

*B. Murphy and T. Miyamoto contributed equally to this paper. Correspondence to Nan Zhang: nzhang@wistar.org.

© 2024 Murphy et al. This article is distributed under the terms of an Attribution–Noncommercial–Share Alike–No Mirror Sites license for the first six months after the publication date (see <http://www.rupress.org/terms/>). After six months it is available under a Creative Commons License (Attribution–Noncommercial–Share Alike 4.0 International license, as described at <https://creativecommons.org/licenses/by-nc-sa/4.0/>).

most abundant cell type found in OvCa tumors and malignant ascites (Charoentong et al., 2017; Izar et al., 2020; Lee et al., 2019; Raghavan et al., 2019; Rickard et al., 2021). The peritoneal cavity consists of at least three anatomical compartments: the peritoneal fluid, the omentum, and the peritoneal membrane. Recent studies have revealed that tissue-resident MΦs in all three compartments can suppress immune responses and promote OvCa progression (Casanova-Acebes et al., 2020; Etzerodt et al., 2020; Long et al., 2021; Miyamoto et al., 2023; Zhang et al., 2021a). Of note, omental MΦs are known to contribute to the formation of the pre-metastatic niche (Etzerodt et al., 2020; Krishnan et al., 2020) and neutrophils recruited to the omentum during early OvCa progression have also been reported to promote metastasis into the omentum (Lee et al., 2019). Therefore, alternative immunotherapy approaches directly targeting myeloid cells in the peritoneal cavity may be necessary to overcome disease progression and resistance.

Nearly a century ago, it was discovered that the administration of dead pathogens (specifically Coley's toxin) could stimulate an antitumor response in some patients, likely via activating myeloid cells that promoted cancer killing (Wiemann and Starnes, 1994). Here, we sought to utilize a similar strategy to treat metastatic OvCa by administering β-glucan alongside IFNγ to activate myeloid cells in the peritoneal cavity. β-glucan is a polysaccharide derived from yeast cell walls and a known activator of myeloid cells. It has been shown to inhibit tumor progression in several non-OvCa tumor models (Bradner et al., 1958; Cheung et al., 2002; Hong et al., 2004; Kalafati et al., 2020; Woeste et al., 2023). Whether it can inhibit metastatic OvCa is not known. IFNγ is an immunogenic cytokine that is essential for innate and adaptive immunity. It was originally identified as an MΦ activation factor (Celada et al., 1984; Schreiber et al., 1982; Svedersky et al., 1984) and is crucial for reprogramming tumor-associated MΦs in multiple tumor models (Alspach et al., 2019; Sun et al., 2021). Importantly, IFNγ alone failed in the most recent clinical trial to improve the prognosis of patients with metastatic OvCa, indicating additional activation signals are necessary (Miller et al., 2009). Both β-glucan and IFNγ are currently in separate clinical trials to investigate efficacy in treating multiple cancers (NCT05159778 and NCT04628338). Importantly, emerging evidence suggests that therapies combining IFNγ and pathogen-derived molecules (e.g., β-glucan or lipopolysaccharide [LPS]) can reverse the immunosuppressive microenvironments in a few clinically relevant, orthotopic cancer models (Sun et al., 2021; Wattenberg et al., 2023). However, whether or how these therapies could treat metastatic OvCa remains poorly understood.

Here, we report that the intraperitoneal administration of β-glucan and IFNγ (BI) successfully induced the robust regression of metastatic OvCa tumors and controlled cancer metastasis. In the peritoneal fluid, we identified two complementary mechanisms through which β-glucan eliminates cancer cells: one that requires macrophage-mediated clotting in the peritoneal fluid and another that requires Dectin-1-Syk-dependent NETosis in the omentum. In solid metastases, we found that both agents for BI treatment are required for tumor regression. BI induced anti-tumor immunity in omentum tumors in part via

MΦ-derived IL27. In vitro, BI directly induced IL27 secretion in MΦs, which consequently activates CD8⁺ T cells. Moreover, we found that higher IL27 expression predicted better overall survival in patients with metastatic OvCa. Overall, this study proposes a new promising therapeutic approach for treating metastatic OvCa and reveals novel mechanisms of tumor control in the peritoneal fluid and omentum tumors.

Results

β-glucan significantly reduces OvCa fluid tumor burden

As β-glucan is a well-known activator of innate immunity and has been reported to control other tumor types in vivo (Bradner et al., 1958; Cheung et al., 2002; Hong et al., 2004; Kalafati et al., 2020; Woeste et al., 2023), we first evaluated whether β-glucan alone could effectively treat tumors in the commonly utilized ID8 mouse model of OvCa. Luciferase- and GFP-tagged ID8 cells were seeded intraperitoneally (i.p.) to simulate metastatic OvCa and mice were treated once every 2 wk with β-glucan (Fig. S1 A). Mouse tumor burden was significantly decreased in β-glucan treated mice (Fig. 1 A). Additionally, malignant ascites (the accumulation of tumor cell- and red blood cell-containing fluid in the peritoneal cavity—a hallmark of metastatic disease) was completely inhibited (Fig. 1 B) and ID8 cells were undetectable in the peritoneal lavage following β-glucan treatment (Fig. 1 C). These data indicate that β-glucan is sufficient to control ID8 tumor progression in vivo.

Although widely utilized for the past 20 years, it is now appreciated that ID8 cells do not harbor any common patient-relevant mutations or somatic copy-number alterations seen in human OvCa (Iyer et al., 2021; Roby et al., 2000; Walton et al., 2016). Therefore, we next wanted to test β-glucan efficacy in another syngeneic model of OvCa that utilizes a recently characterized cell line containing OvCa patient-relevant genetic alterations, KPCA (KRAS^{G12V}Trp53^{R172H}CCNE1^{OE (OE)}Akt2^{OE}, Fig. 1 D) (Iyer et al., 2021). KRAS, TP53, CCNE1, and AKT2 are mutant alleles observed in high-grade serous ovarian tumors with frequencies of 12%, 96%, 19%, and 6%, respectively (Iyer et al., 2021; Zhang et al., 2021b). Interestingly, the amplification of KRAS and CCNE1 was recently identified as a marker for chemoresistant OvCa (Smith et al., 2023) and these tumors were indeed reported to be resistant to chemotherapy (Iyer et al., 2021). Therefore, utilizing this model is valuable for developing effective therapies against therapy-resistant OvCa in patients, an unmet clinical need.

Mice bearing KPCA tumors have a median survival of only 35 days, which is a nearly threefold decrease compared to the ID8 model which has a median survival of 114 days (Iyer et al., 2021; Roby et al., 2000). To account for this, treatment was initiated 1 wk following KPCA injection, and mice were treated with two doses of β-glucan on days 7 and 14 (Fig. S1 B). We confirmed the presence of KPCA cells (GFP⁺luciferase⁺) in the peritoneal fluid (Fig. 1 E and Fig. S1 C) as well as in the omentum at the time of treatment initiation (Fig. 1 F; and Fig. S1, D and E), which models metastatic OvCa (stage III or IV) in patients (Prat, 2014). For reasons that are not known, KPCA cells lose their luminescence in the peritoneal fluid. Therefore, a bioluminescent signal is indicative of solid tumor burden only and fluid tumor burden was exclusively analyzed by flow cytometric enumeration of GFP⁺

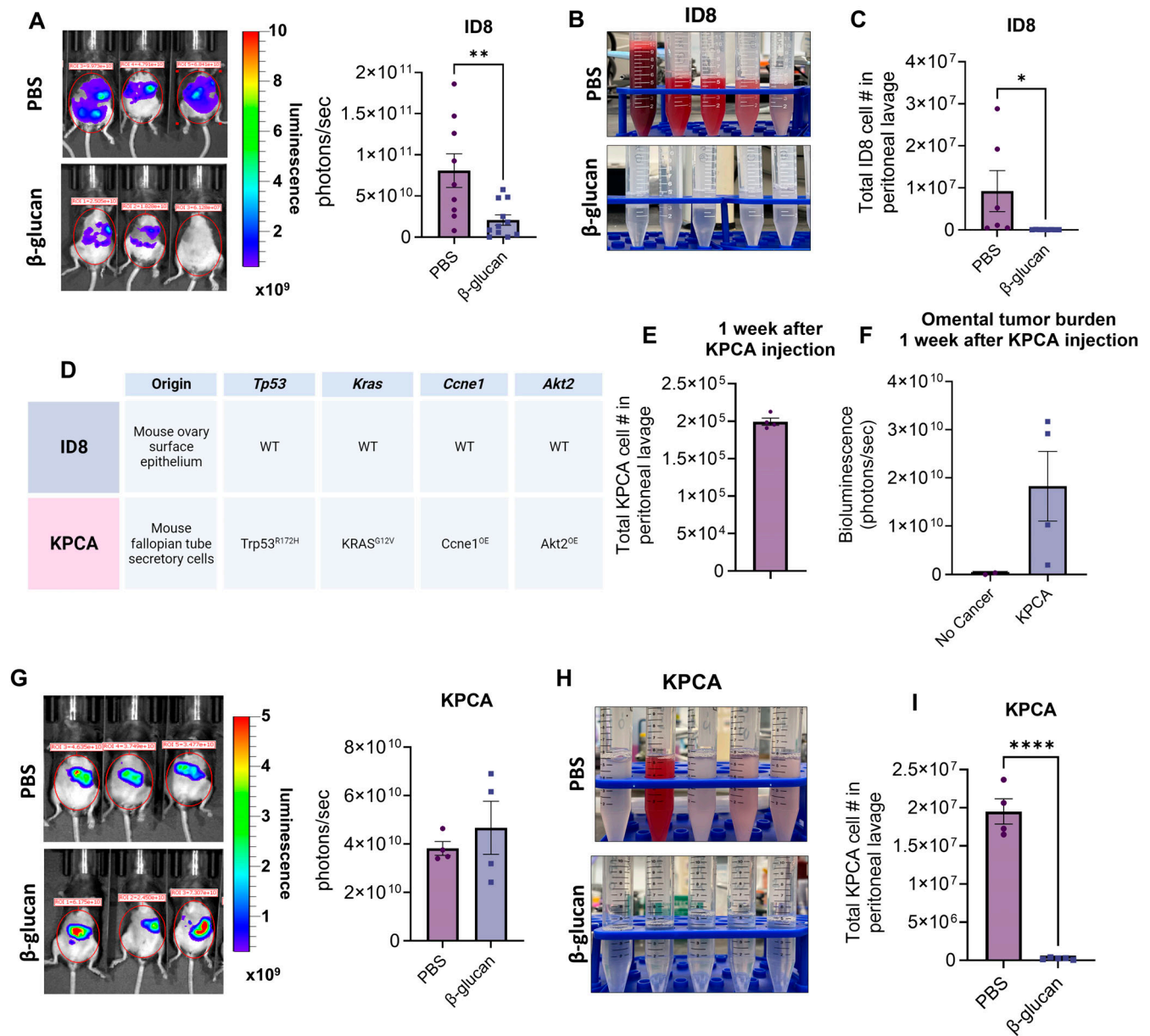


Figure 1. β-glucan significantly reduces OvCa fluid tumor burden. (A) Representative bioluminescence images and quantification of bioluminescence signals in PBS- and β-glucan-treated ID8 tumor-bearing mice 42 days after tumor seeding. (B and C) (B) Representative pictures of peritoneal lavage and (C) quantification of GFP⁺ ID8 OvCa cells in the peritoneal lavage of PBS- and β-glucan-treated mice. (D) Tissue of origin and mutation status of *Tp53*, *Kras*, *Ccne1*, and *Akt2* in ID8 and KPCA OvCa cell lines. (E) Quantification of KPCA cells in the peritoneal lavage 1 wk after KPCA seeding. (F) Quantification of omentum bioluminescence signals 1 wk after KPCA seeding. (G) Representative bioluminescence images and quantification of bioluminescence signals in PBS- and β-glucan-treated KPCA tumor-bearing mice. (H and I) (H) Representative pictures of peritoneal lavage and (I) quantification of GFP⁺ KPCA OvCa cells in the peritoneal lavage in PBS- and β-glucan-treated mice. Data from three independent runs combined and presented in bar graphs. Each dot represents one mouse. Student's t test was used *P < 0.05; **P < 0.01; ****P < 0.0001. Error bars are standard errors of the mean.

cells. In contrast to ID8 tumors, β-glucan could not reduce the KPCA solid tumor burden (Fig. 1 G). However, β-glucan once again was able to inhibit the accumulation of malignant ascites (Fig. 1 H and Fig. S1 F) and significantly reduced KPCA cell number in the peritoneal lavage (Fig. 1 I). Taken together these data suggest that β-glucan is sufficient to control fluid tumor burden independent of tumor type. However, β-glucan was unable to control the metastatic growth of KPCA tumors. The ability of β-glucan to control solid tumor progression of ID8 tumors but not KPCA further

highlights the critical role of tumor mutation status on therapy response and emphasizes the importance of utilizing preclinical models which better model human cancer.

β-glucan captures ovarian cancer into solid nodular structures via intraperitoneal clotting and Dectin-1-Syk-dependent NETosis in the omentum

Given that β-glucan significantly reduced the presence of cancer cells in the ascites of tumor-bearing mice, we next sought to

determine the mechanism by which β -glucan eliminates cancer cells from the peritoneal fluid.

One distinguishing characteristic of peritoneal resident macrophages (PRM Φ s) is their ability to rapidly aggregate around foreign particles or pathogens, entrapping them in clot-like structures and facilitating their clearance from the peritoneal fluid (Barth et al., 1995). This process is known as the M Φ disappearance reaction (MDR) and is critical to control infection in the peritoneal cavity (Vega-Pérez et al., 2021; Zhang et al., 2019). To test whether MDR could be responsible for the disappearance of cancer cells from the peritoneal fluid, we administered GFP-labeled OvCa cells concurrently with β -glucan and analyzed peritoneal lavage 5 h later (Fig. S2 A). We first confirmed MDR in our model by observing the disappearance of PRM Φ s (F4/80^{hi}CD11b^{hi}ICAM2^{hi}) in the peritoneal fluid following β -glucan administration (Fig. 2 A). We next looked for the presence of GFP⁺ cancer cells in the peritoneal fluid to see if they also disappeared. Indeed, the presence of both ID8 cells (Fig. S2 B) and KPCA cells (Fig. 2 B and Fig. S2 C) was significantly reduced in β -glucan-treated mice. Because cancer cell disappearance does not appear to be dependent on cell type, KPCA cells were used for the remaining experiments. Similar to what has been previously reported in infection models, clot-like structures also formed in our cancer model following β -glucan treatment. These structures could be visualized as ~1–2 mm GFP⁺ clots freely floating in the peritoneal cavity (Fig. 2 B and Fig. S2 D) and flow cytometric analysis of these structures confirmed the presence of CD45⁺GFP⁺ KPCA cells within (Fig. 2 D), thus suggesting that MDR can indeed capture cancer cells in the peritoneal fluid. To confirm this, we examined the peritoneal lavage of mice treated with clodronate-loaded liposomes (CLL), which deplete PRM Φ s (Fig. S2 E) (van Rooijen and Hendriks, 2010). Indeed, KPCA disappearance was partially impaired in CLL-treated mice (Fig. S2 F). Moreover, concurrent administration of β -glucan with heparin, an anticoagulant which inhibits MDR by disrupting PRM Φ clotting (Zhang et al., 2019), also partially impaired KPCA disappearance in the peritoneal lavage (Fig. 2 E). Finally, OvCa cells captured within these clots were more apoptotic than untreated cancer cells freely floating in the peritoneal fluid as determined by TUNEL staining analyzed by flow cytometry (Fig. S2 G). Taken together, these data confirm that intraperitoneal administration of β -glucan can capture OvCa cells floating in the peritoneal fluid into clot-like structures by activating MDR, leading to sequestration of OvCa cells out of the peritoneal fluid.

We next wanted to investigate the molecular mechanism underpinning β -glucan-mediated cancer removal from the peritoneal fluid. Dectin-1, a C-type lectin receptor expressed by myeloid cells, recognizes β -glucan and signals via downstream spleen tyrosine kinase (Syk) (Brown et al., 2002). To determine the contribution of Dectin-1-Syk signaling in cancer cell disappearance, we first analyzed the peritoneal lavage of mice with Syk-deficient myeloid cells (Syk^{Mye Δ}). Indeed, the disappearance of cancer cells from the fluid was impaired in Syk^{Mye Δ} mice as compared to their littermate controls (Syk^{WT}, Fig. 2 F). Surprisingly, impaired OvCa cell disappearance occurred independent of MDR as PRM Φ s were still undetectable in the peritoneal

lavage of Syk^{Mye Δ} mice after β -glucan treatment (Fig. 2 G). Moreover, neither Syk deficiency nor MDR inhibition completely reversed OvCa cell removal from the peritoneal fluid (Fig. 2, E and F), thus implying the existence of two independent cancer sequestration mechanisms: one which involves MDR and another which requires Syk signaling in myeloid cells.

The omentum is an immune-rich adipose tissue which is critical for clearing peritoneal contaminants and coordinating protective immune responses during peritonitis (Català et al., 2022; Meza-Perez and Randall, 2017). Notably, zymosan (a type of β -glucan) has been reported to be rapidly sequestered into the omentum following i.p. injection (Jackson-Jones et al., 2020). Therefore, to further elucidate the MDR-independent, Syk-dependent mechanism of cancer clearance, we examined the omentum in β -glucan-treated mice. To test whether the omentum can capture OvCa cells following intraperitoneal β -glucan administration, we imaged the omentum in situ 5 h following KPCA cell and β -glucan injection. Mouse body cavities were opened, and the omentum was gently stretched across the liver to ensure low background fluorescence and clear imaging. Green fluorescing OvCa cells were clearly visualized in the omentum following β -glucan treatment (Fig. 2 H), indicating that the omentum can indeed sequester OvCa cells following β -glucan administration. Moreover, OvCa cell disappearance from the peritoneal lavage was partially but significantly reversed in mice whose omentum was surgically removed by omentectomy (OMX, Fig. 2 I). Like what was observed in Syk^{Mye Δ} mice, reversal of OvCa cell disappearance occurred in OMX mice independent of MDR (Fig. S2 H), thus supporting the notion that sequestration by the omentum and MDR likely occurs independently of one another. To confirm this, we administered heparin in OMX mice where both MDR and omentum capture were inhibited, and observed cancer cell disappearance from the peritoneal fluid was completely reversed in these mice (Fig. 2 I). This supports the existence of two complementary pathways in two independent structures (clots formed in the peritoneal fluid and the omentum) that are required for total OvCa cell sequestration by β -glucan.

Given that cancer cell disappearance in Syk^{Mye Δ} mice phenocopied what was observed in OMX mice, we next wanted to test whether Dectin-1-Syk signaling could drive cancer cell sequestration in the omentum. Indeed, fewer cancer cells were observed in the omentum of Syk^{Mye Δ} mice as seen by imaging and flow cytometry (Fig. 2 J and Fig. S2 I). Moreover, like OMX mice, heparin administration in Syk^{Mye Δ} and constitutive Dectin-1 knockout mice (Dectin-1 KO) once again completely reversed OvCa cell disappearance in the peritoneal lavage (Fig. 2, K and L). Moreover, depletion of M Φ s using CLL in Syk^{Mye Δ} mice also completely reversed OvCa cell disappearance (Fig. S2 J), further confirming that Dectin-1-Syk signaling drives OvCa cell capture in the omentum independent of MDR.

Finally, we sought to identify the mechanism through which OvCa cells were trapped within the omentum. A recent report demonstrated that the capture of zymosan in the omentum is mediated by neutrophil recruitment and activation of neutrophil extracellular traps (NETs) (Jackson-Jones et al., 2020). Additionally, Syk signaling has been reported to be a master

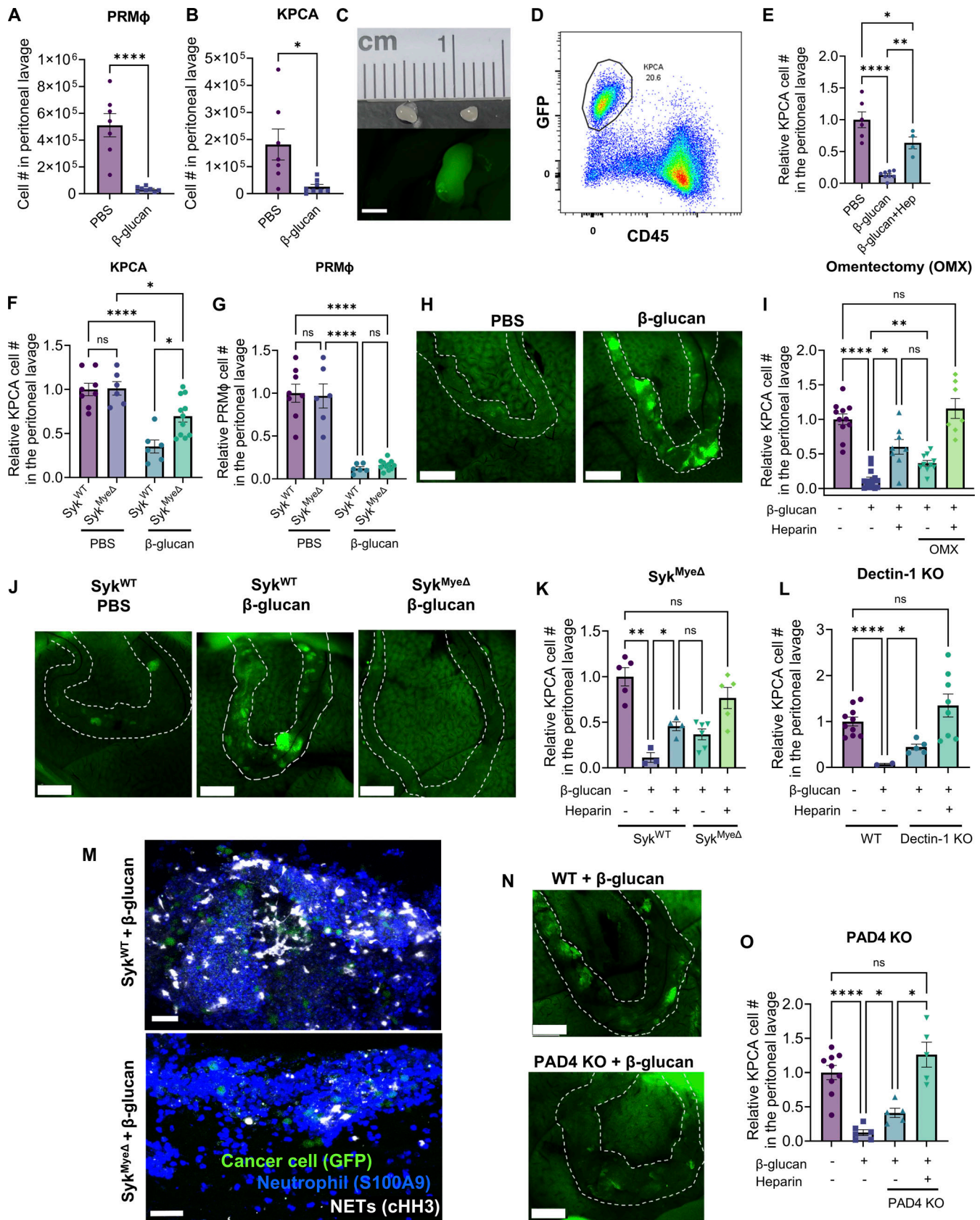


Figure 2. **β-glucan captures OvCa cells into solid nodular structures via intraperitoneal clotting and Dectin-1-Syk-dependent NETosis in the omentum.** (A and B) Quantification of (A) PRMφ and (B) KPCA cells in the peritoneal lavage of mice 5 h following PBS or β-glucan treatment. (C and D) (C) Representative image and (D) flow plot of peritoneal clots formed in the peritoneal fluid following β-glucan treatment containing GFP+CD45⁻ KPCA cells.

(E) Quantification of PRMΦ and KPCA cells in the peritoneal lavage 5 h after PBS, β-glucan, and β-glucan+heparin treatment. **(F and G)** Quantification of (F) KPCA and (G) PRMΦ in the peritoneal lavage of Syk^{WT} and Syk^{MyeΔ} mice treated with PBS or β-glucan. **(H)** Representative images of omentum in mice 5 h after PBS and β-glucan treatment. Omentum was stretched over the liver for better imaging. **(I)** Quantification of KPCA cells in the peritoneal lavage in intact and OMX mice treated as indicated with PBS, β-glucan, and heparin. **(J)** Representative images of omentum in Syk^{WT} and Syk^{MyeΔ} mice 5 h after β-glucan treatment. **(K and L)** Quantification of KPCA in the peritoneal lavage of (K) Syk^{MyeΔ} and (L) Dectin-1 KO mice 5 h following treatment as indicated with PBS, β-glucan, and heparin. **(M)** representative confocal images of omentum of Syk^{WT} and Syk^{MyeΔ} mice 5 h after β-glucan treatment. Positive cells were stained blue (S100A9; neutrophil), green (GFP; cancer cell), and white (cHH3; NETs). **(N and O)** (N) Representative images of omentum, and (O) quantification of KPCA cells in peritoneal lavage in WT and PAD 4KO mice 5 h after indicated treatment. Data from three or more independent runs combined and presented. Each dot represents one mouse. One-way ANOVA and Student's *t* test were used. **P* < 0.05; ***P* < 0.01; *****P* < 0.0001. Error bars are standard errors of the mean. Relative cell number is reported as a fold change to the average of the control and was used when experimental replicates were combined. Scale bar is 1 mm for panel C, 2 mm for panels H, J, and M, and 50 μM for panel M.

regulator of NETosis in response to β-glucan (Nani et al., 2015; Negoro et al., 2020; Zhu et al., 2023). Given that Syk signaling in myeloid cells is crucial for OvCa cell capture in the omentum, we posited that OvCa cells could be captured via Syk-dependent NETosis in the omentum. Whole-mount confocal imaging of the omentum 5 h after β-glucan and KPCA administration demonstrated that NETs, marked by citrullinated histone H3 (cHH3), were indeed induced by β-glucan and localized with neutrophils and OvCa cells in the omentum (Fig. 2 M). Moreover, this signal decreased in Syk^{MyeΔ} mice (Fig. 2 M), confirming that Syk-mediated NETosis may drive OvCa cell capture by the omentum. Finally, we found that inhibiting NETs directly by genetically deleting peptidyl arginine deiminase type IV in mice (PAD4 KO) (Li et al., 2010) reversed OvCa cell capture by the omentum (Fig. 2 N) and that adding heparin in PAD4 KO mice once again fully reversed OvCa cell disappearance from the peritoneal lavage (Fig. 2 O). Thus, β-glucan induces the capture of OvCa cells by the omentum via Dectin-1-Syk-mediated NETosis.

Taken together, we identified two nonredundant yet complementary pathways that mediate sequestration of disseminating OvCa cells from the peritoneal fluid by β-glucan: (1) an MDR-mediated intraperitoneal clotting mechanism in the peritoneal fluid and (2) a Dectin-1-Syk-dependent NETosis mechanism in the omentum. A simplified illustration of these pathways can be found in Fig. S2 K.

Combining β-glucan with IFNγ reduces KPCA tumor burden through host immunity

Although β-glucan treatment alone effectively controlled fluid tumor burden, it was unable to control metastatic growth of KPCA tumors in vivo (Fig. 1 H). Emerging evidence suggests that therapies combining IFNγ and pathogen-derived molecules can be utilized against cancers and have been tested in a few clinically relevant, orthotopic cancer models (Sun et al., 2021; Wattenberg et al., 2023). In light of this, we adopted a similar approach and posited that β-glucan in combination with IFNγ could potentially treat KPCA tumors.

To test the efficacy of BI against KPCA tumors, 1×10^6 luciferase-tagged KPCA cells were seeded i.p. and treated as shown in Fig. 3 A. BI significantly reduced KPCA tumor burden as visualized by bioluminescence imaging, flow cytometry, and omentum weight (Fig. 3 B; and Fig. S3, A and B), but single-agent β-glucan or IFNγ did not. Reduction of KPCA tumor burden was completely impaired in IFNγ receptor KO mice (IFNγR KO, Fig. 3

C) and BI treatment did not reduce KPCA number in vitro (Fig. S3 C), indicating that the therapy is not directly cytotoxic to tumors but requires cancer-extrinsic IFNγR-mediated host immune responses. MΦ activation can promote tumor killing by activating T cells (Sun et al., 2021). To test whether T cells are required for the antitumor activity of BI, we depleted T cells in vivo using monoclonal antibodies against CD4 and CD8 (αCD4+αCD8). Indeed, mice lacking CD4⁺ and CD8⁺ T cells are unable to control tumor burden following BI (Fig. 3 D). Taken together, these data indicate that BI activates host immunity to robustly control metastatic KPCA tumors in vivo.

We next sought to determine whether BI could drive tumor regression. To this end, we tracked tumor growth longitudinally following treatment via bioluminescence imaging (Fig. S3 D). Notably, there was no difference in tumor burden across all treatment groups on days 8, 10, or 14; however, there was a significant decrease in tumor burden in only BI-treated mice on day 21 (Fig. 3, E and F; and Fig. S3 E). These data indicate that BI may induce direct tumor killing and disease regression, although it does not rule out the possibility that BI may reduce tumor growth. Compartmental imaging of the omentum and the non-omentum body cavity (Fig. S1 D) revealed that the omentum had the greatest tumor burden in untreated mice. Compartmental imaging of BI-treated mice revealed that both β-glucan and IFNγ were required to control tumors in the omentum (Fig. 3 G) as well as throughout the rest of the cavity (Fig. 3 H). Moreover, ascites accumulation was once again eradicated in both β-glucan- and BI-treated mice (Fig. S3, F and G). To test the toxicity of BI, we performed a complete clinical chemistry panel with IDEXX and analyzed multiple organ damage markers in the serum of mice on day 21. Of the 14 parameters measured, only a change in phosphorous levels reached statistical significance (*P* = 0.0020, Fig. S3 H) being decreased in the serum of BI-treated mice as compared to PBS-treated. However, AST, ALT, alkaline phosphatase, and creatine kinase concentrations trended up while bilirubin and blood urea nitrogen levels trended down in BI-treated mice as compared to PBS-treated mice (Fig. S3 H). Finally, there was no difference in body weight between PBS- and BI-treated mice (Fig. S3 I). These data suggest that two rounds of BI treatment may induce some insignificant amount of toxicity in mice; however, a more thorough toxicity study is warranted prior to testing in humans.

Taken together, these data demonstrate that BI activates host immunity to robustly kill KPCA tumors in metastatic sites in the peritoneal cavity in vivo.

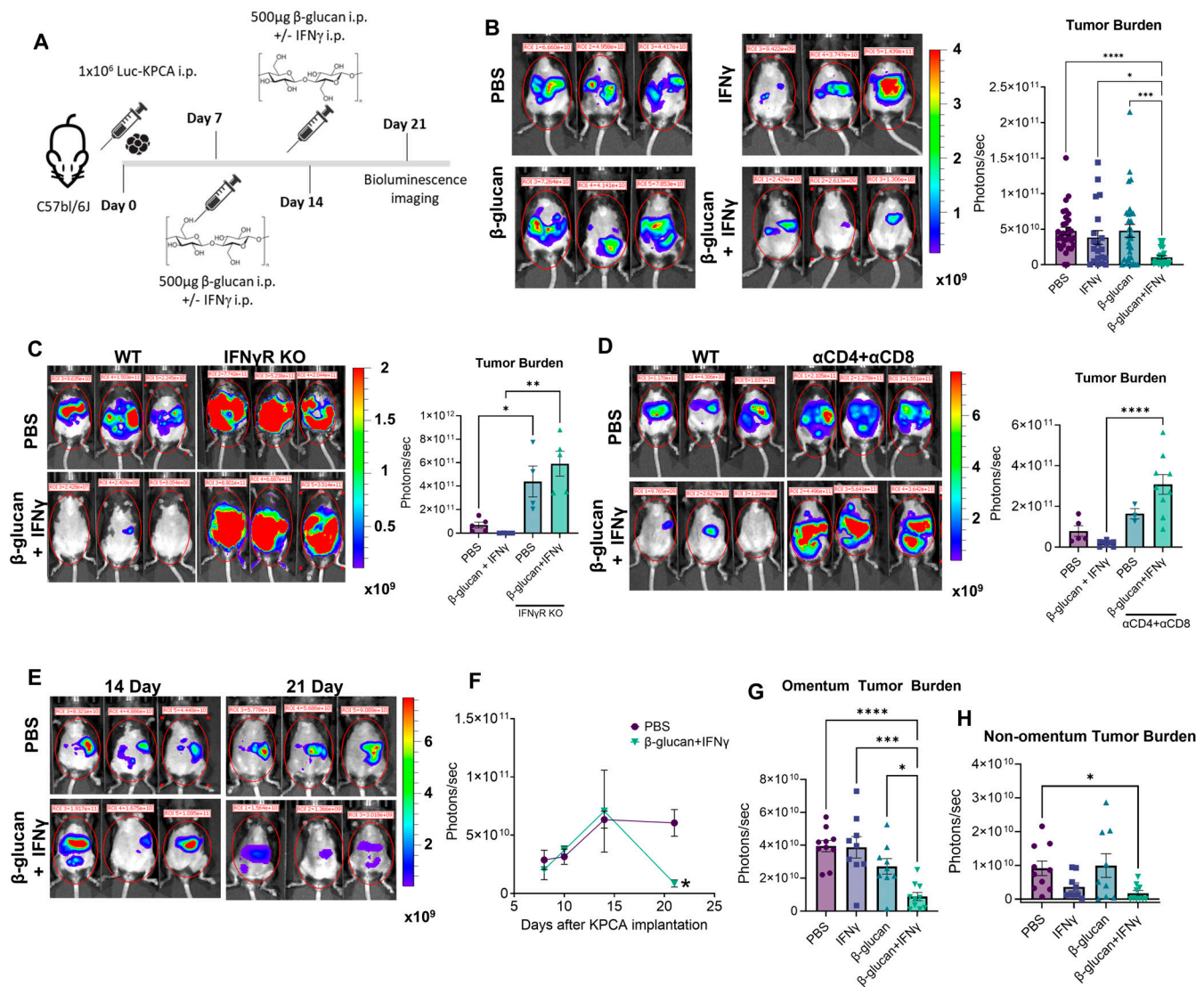


Figure 3. Combining β -glucan with IFN γ reduces KPCA tumor burden through host immunity. (A) BI timeline in KPCA model of OvCa. (B) Representative bioluminescence images and quantification of bioluminescent signal in mice treated with PBS, IFN γ , β -glucan, or BI. (C and D) Representative bioluminescence images and quantification of bioluminescent signal in (C) IFN γ R KO mice and (D) T cell-depleted mice treated with PBS or BI. (E and F) Representative bioluminescence images and (F) quantification of bioluminescent signal of PBS and BI-treated mice on days 8, 10, 14, and 21. (G and H) (G) Omentum and (H) non-omentum body cavity bioluminescent signal in PBS-, IFN γ -, β -glucan-, or BI-treated mice. Data from two or more independent runs combined and presented in bar graphs. Each dot represents one mouse. One-way ANOVA and Student's *t* test were used. **P* < 0.05; ***P* < 0.01; ****P* < 0.001; *****P* < 0.0001. Error bars are standard errors of the mean.

BI enriches IL27⁺ antitumor M Φ s in omentum tumors

BI can signal through receptors expressed by M Φ s (Dectin-1 and IFN γ R, respectively). To test whether M Φ s are required for BI-induced antitumor immunity, we depleted M Φ s using CLL during the course of BI treatment and found that mice treated with CLL had a higher tumor burden than BI+PBS-treated mice (Fig. 4 A), suggesting that M Φ s are required for the optimal tumor control induced by BI.

Next, we sought to investigate how M Φ s facilitated antitumor immunity. We focused on omentum tumors because they were the largest tumor burden and very few tumor nodules were present in any other peritoneal compartment or the fluid following BI (Fig. 3, G and H). Flow cytometric analysis of

omentum tumors revealed a reduction in pro-tumor Arginase-1⁺ and Tim-4⁺ M Φ s (Fig. S4 A), which have been reported to promote tumor progression by suppressing T cell functions (Noy and Pollard, 2014; Xia et al., 2020). To determine whether there is a unique subset of monocytes/M Φ s which may promote antitumor activity, we performed scRNA-seq on omentum tumors and identified eight clusters of monocytes/M Φ s (Fig. 4, B and C). Using the Immunological Genome Project dataset as a reference, Clusters 1 and 5 were identified as monocytes; all other clusters were identified as M Φ s. Notably, Cluster 2 frequency was selectively enriched in BI-treated mice, while Cluster 1 was reduced (Fig. 4 D). Cluster 1 monocytes selectively expressed inflammation-related genes such as *Il1b* and *Vcan*, whereas

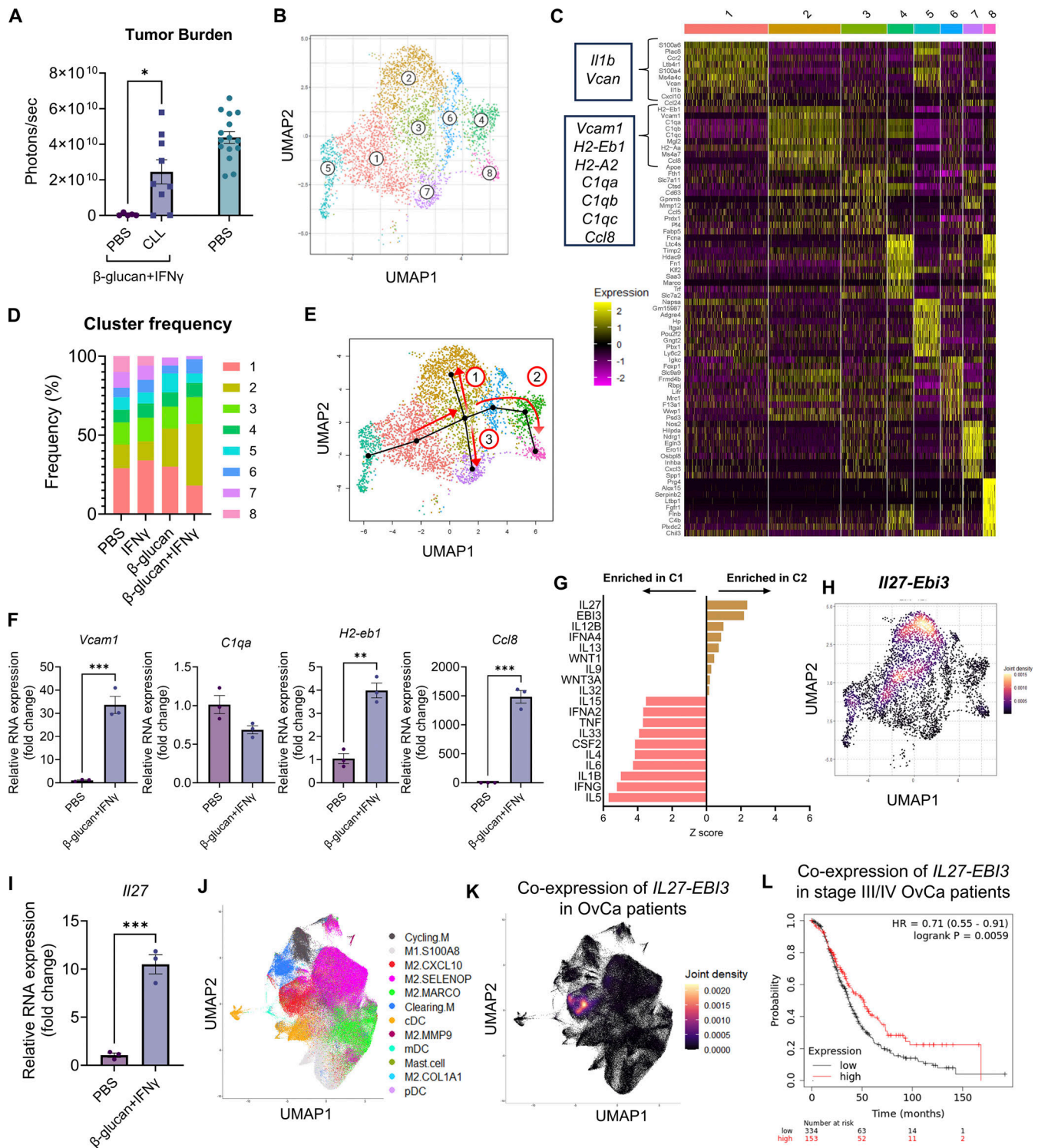


Figure 4. **BI enriched IL27⁺ macrophages in omentum tumors.** (A) Whole body bioluminescent signal of PBS or CLL-treated mice treated with BI and control mice. (B) A UMAP plot of monocyte/MΦ clusters in omentum tumors. (C) Top upregulated genes in all monocyte/MΦ clusters. (D) Frequencies of eight identified monocyte/MΦ clusters in omentum tumors. (E) Slingshot trajectory analysis from the origin (cluster 5) through three independent pathways (red arrows). (F) qPCR analysis of cluster genes in monocyte-derived MΦs treated with PBS or BI. (G) Top upregulated IPA cytokine regulators in clusters 1 and 2. (H) *IL27* and *Ebi3* co-expression heatmap of monocyte/MΦ clusters. (I) *IL27* expression in monocyte-derived MΦs treated with PBS or BI analyzed by qPCR. (J and K) (J) Uniform manifold approximation and projection (UMAP) plot of monocyte/MΦ clusters and (K) *IL27* and *EBI3* co-expression in tumors from human OvCa patients. (L) Overall survival analysis in late-stage OvCa patients (stage III and IV) with high and low co-expression of *IL27-EBI3*. Data from two or more independent runs combined and presented in bar graphs. Each dot represents one mouse. Student's *t* test was used. **P* < 0.05; ***P* < 0.01; ****P* < 0.001. Error bars are standard errors of the mean.

Cluster 2 MΦs were enriched with genes related to antigen presentation (*H2-Aa*, *H2-Eb1*), immune activation (*Ccl8*, *Vcam1*), and complement activation (*Clqa*, *Clqb*, *Clqc*) (Fig. 4 C).

To better understand the origin and development of Cluster 2 MΦs we performed Slingshot trajectory analysis of our single-cell RNA sequencing (scRNA-seq) dataset. Setting Cluster 5 monocytes as the origin, we found three distinct differentiation pathways (Fig. 4 E). All trajectories passed from Cluster 5 through Clusters 1 and 3 before diverging and terminating in Clusters 2, 7, and 8. These data suggest that Cluster 2 MΦs developed from monocytes through a unique pathway. To support this hypothesis, we cultured monocytes isolated from bone marrow and stimulated them with BI during their in vitro differentiation into MΦs. MΦs that differentiated in the presence of BI upregulated multiple markers of Cluster 2 MΦs, such as *Vcam1*, *H2-eb1*, and *Ccl8*, but not *Clqa* (Fig. 4 F). Additionally, we investigated whether BI could systematically augment immune progenitors and monocytes in vivo. To this end, we analyzed bone marrow cells by flow cytometry 1 wk after BI treatment and found that Lin-Sca1+cKit progenitor cells, long-term hematopoietic stem cells, multipotent progenitor cells, and Ly6C^{hi} monocytes were all increased in number compared to PBS-treated mice (Fig. S4 B). Taken together, these data suggest that Cluster 2 MΦs develop from bone marrow monocytes but require additional signals in the tumor microenvironment to mature fully.

To understand what signals Cluster 2 MΦs may upregulate to activate T cells to drive an antitumor response, we chose to focus on MΦ-derived cytokines, which are key approaches MΦs use to activate T cells. Ingenuity pathway analysis (IPA) specifically focusing on cytokine regulators in Cluster 1 and 2 confirmed the pro-inflammatory phenotype of Cluster 1 monocytes as inflammatory cytokine pathways were highly enriched, such as IL1β and IL6 (Fig. 4 G). In contrast, both subunits of the IL27 cytokine heterodimer (IL27 and EBI3) were significantly enriched in Cluster 2 (Fig. 4 G), and *Il27* and *Ebi3* co-expression was predominately detected in Cluster 2 MΦs (Fig. 4 H). Moreover, monocyte-derived MΦs in the presence of BI expressed higher levels of *Il27* when compared to untreated MΦs (Fig. 4 I). IL27 is an unconventional IL12-family cytokine that has both pro- and antitumor properties depending on tumor types (Fabbi et al., 2017; Yoshida and Hunter, 2015), while IL12 is the classical MΦ-derived antitumor cytokine (Chan et al., 1991; Kaczanowska et al., 2021). Surprisingly, IL12 was almost undetectable in any of our MΦ subpopulations (Fig. S4 C).

Lastly, to determine whether IL27 signaling is relevant in OvCa patients, we analyzed a recently published scRNA-seq dataset of tumors and ascites from patients with metastatic OvCa (Vázquez-García et al., 2022). In these tumors, *Il27* and *Ebi3* were exclusively co-expressed in only monocytes/MΦs (Fig. S4, D and E), specifically in the “M2.CXCL10” subset (Fig. 4, J and K). To our surprise, we did not find significant expression of IL12 in these tumor samples (Fig. S4 F), consistent with the result from our mouse model. Finally, utilizing public datasets, we analyzed the correlation between overall patient survival and IL27 expression. Indeed, higher co-expression of *Il27* and *Ebi3* significantly correlated with improved survival in patients with stage III/IV metastatic OvCa (Fig. 4 L, $P = 0.0059$). In

summary, these results suggest that BI treatment causes regression of metastatic OvCa by promoting differentiation of monocytes into IL27⁺ antitumor MΦs.

IL27 contributes to BI treatment by activating T cells and is specifically secreted by BI-stimulated MΦs

To test whether IL27 contributes directly to the antitumor response of BI, we neutralized IL27 using a monoclonal antibody against IL27p28 in the presence of BI in vivo. Indeed, IL27 neutralization significantly impaired the antitumor activity in both omental and mesenteric metastases as compared to IgG controls (Fig. 5, A and B). Given the requirement of T cells for BI efficacy (Fig. 3 D), we next evaluated changes in T cells following BI treatment and examined the potential role of IL27 underlying these responses. T cells from PBS- and BI-treated omentum tumors were restimulated ex vivo and analyzed by flow cytometry. T cells secrete cytokines such as IFNγ and TNF upon activation to drive anti-tumor immune responses. In BI-treated tumors, although CD8⁺ T cell frequencies did not change (Fig. S5 A), IFNγ⁺ and TNF⁺ CD8⁺ T cells were enriched (Fig. S5 B) and IFNγ and TNF mean fluorescent intensity (MFI) was increased (Fig. 5 C). Interestingly, in CD4⁺ T cells, only the frequency of TNF⁺ was increased, and no other significant changes were observed (Fig. S5 C). Therefore, BI treatment is immunostimulatory and its efficacy likely relies on the activation of CD8⁺ cytotoxic T cells.

To test whether MΦ-derived IL27 contributes to the immunostimulatory effect seen in BI treatment, we established an in vitro system using MΦs and CD8⁺ T cells. First, to test whether the IL27 can be directly secreted from MΦs stimulated by BI, we treated bone marrow-derived MΦs (BMDMs) with BI for 48 h and tested the supernatant for secreted IL27 using an IL27/EBI3 heterodimer-specific ELISA. Interestingly, while β-glucan alone can generate a small amount of IL27, both β-glucan and IFNγ are required for robust IL27 secretion (Fig. 5 D). It has been previously reported that the p28 subunit of IL27 (also known as IL30 when IL27p28 forms a monomer) can be generated in MΦs stimulated with IFNγ or LPS (another pathogen-associated molecular pattern [PAMP] molecule) as detected by an IL27p28 ELISA (not specific for IL27 heterodimer). In this context, a single agent is sufficient to induce IL27p28 production, but combining the two agents synergizes to produce a maximal amount of IL27p28 (Liu et al., 2007). Notably, we see a similar pattern in IL27p28 secretion in BMDMs treated with β-glucan or IFNγ (Fig. S5 D). Therefore, secretion of the IL27 heterodimer is specific to BI treatment despite IL27p28 generation induced by single agents, suggesting that both agents may be necessary for the transcription of EBI3, but how this occurs remains unknown. Surprisingly, IL27 did not require Dectin-1-Syk signaling as BMDMs from Dectin-1 KO and Syk^{MyeΔ} mice still secreted IL27 following BI treatment (Fig. 5 E). On the other hand, IFNγR was crucial for IL27 production as loss of this receptor completely ablated IL27 secretion in BMDMs (Fig. 5 E). Therefore, we show that secretion of the IL27 heterodimer is a specifically regulated event which requires IFNγ receptor signaling but not Dectin-1 or Syk. Given the role IL27 plays in BI efficacy (Fig. 5 A), the specific generation of IL27 by BI may offer one explanation as to why single agent β-glucan or IFNγ

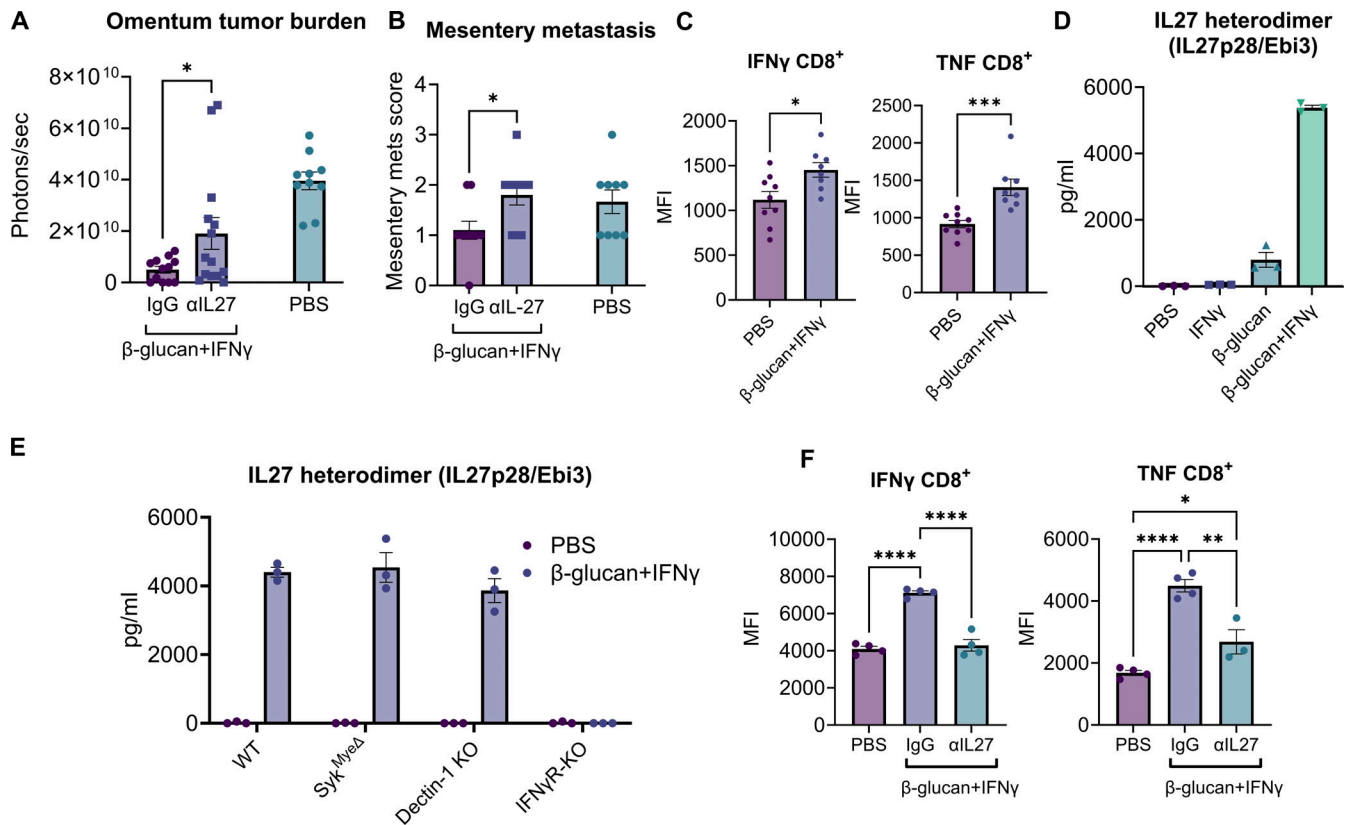


Figure 5. IL27 contributes to BI treatment by activating T cells and is specifically secreted by BI-stimulated MΦs. (A and B) (A) Bioluminescent signal of omentum tumors and (B) mesentery metastasis scores from mice injected with IgG or αIL27 treated with BI and untreated control mice. **(C)** MFI of IFN γ and TNF in CD8⁺ T cells in omentum tumors for control or BI-treated mice analyzed by flow cytometry. **(D)** ELISA quantification of IL27 heterodimer in supernatant from BMDM stimulated with PBS, IFN γ , β-glucan, or BI. **(E)** ELISA quantification of IL27 heterodimer in supernatant from WT-, Syk^{MyeΔ}, Dectin-1 KO, and IFN γ R-KO-BMDM cultured with PBS or BI. **(F)** IFN γ and TNF MFI of CD8⁺ T cells cocultured with MΦ pretreated with PBS or BI in the presence of αIL27 antibody or control IgG. In vivo data combined from three independent runs plotted where each dot represents one mouse. One representative run presented for in vitro data where each dot represents one replicate. Experiment replicated at least three times. Student's *t* test and one-way ANOVA were used. **P* < 0.05; ***P* < 0.01; ****P* < 0.001; *****P* < 0.0001. Error bars are standard errors of the mean.

treatment was not sufficient in controlling OvCa tumor burden (Fig. 3 B).

To test whether MΦ-derived IL27 could drive the immunostimulatory phenotype in CD8⁺ T cells, naïve OT-I CD8⁺ T cells were co-cultured with PBS- or BI-pretreated BMDMs, OVA peptide, and dendritic cells (DCs) in the presence of control or an IL27p28 neutralization antibody. Indeed, co-culturing T cells with BI-pretreated BMDMs increased the frequency of IFN γ ⁺, TNF⁺, and IFN γ ⁺TNF⁺ CD8⁺ T cells (Fig. S5, E and F) and increased IFN γ and TNF MFI (Fig. 5 F) in an IL27-dependent manner. BI-pretreated MΦs also increased Granzyme B expression (a cytotoxic effector molecule in CD8⁺ T cells) but did so independently of IL27 (Fig. S5 G). Taken together, these data suggest that BI treatment directly stimulates IL27 expression in MΦs and that MΦ-derived IL27 promotes the anti-tumor activity of BI treatment via activating cytotoxic CD8⁺ T cells.

BI extends overall survival in both chemoresistant and chemo-sensitive models and dramatically enhances chemotherapy response in the chemo-sensitive model

To test whether βI can be combined with platinum-based chemotherapy (standard-of-care for OvCa patients) to treat

metastatic OvCa, we treated the homologous recombination (HR)-proficient chemoresistant KPCA and HR-deficient chemosensitive BPPNM (*p53*^{-/-R172H}*Brca1*^{-/-Pten}^{-/-Nfl}^{-/-Myc}^{OE}) tumors (Iyer et al., 2021) with BI once a week for 2 wk with or without carboplatin and monitored their overall survival. As expected in the chemoresistant KPCA model, carboplatin alone did not yield any survival advantage compared to PBS controls, but BI significantly extended the overall survival and led to the survival of 20% of mice at the end of the study. In addition, combining BI with carboplatin did not lead to a survival advantage compared to BI alone. On the other hand, in the HR-deficient chemo-sensitive BPPNM model, carboplatin alone significantly extended the overall survival, while BI modestly prolonged the survival (Fig. 6 B). In sharp contrast to the KPCA model, combining BI with carboplatin led to 80% of mice alive at the end of the study in mice carrying BPPNM tumors (Fig. 6 B). These results suggest that combining BI with platinum-based chemotherapy may yield a significant therapeutic advantage compared to chemotherapy alone in HR-deficient OvCa, while BI may be a treatment option for chemoresistant HR-proficient OvCa.

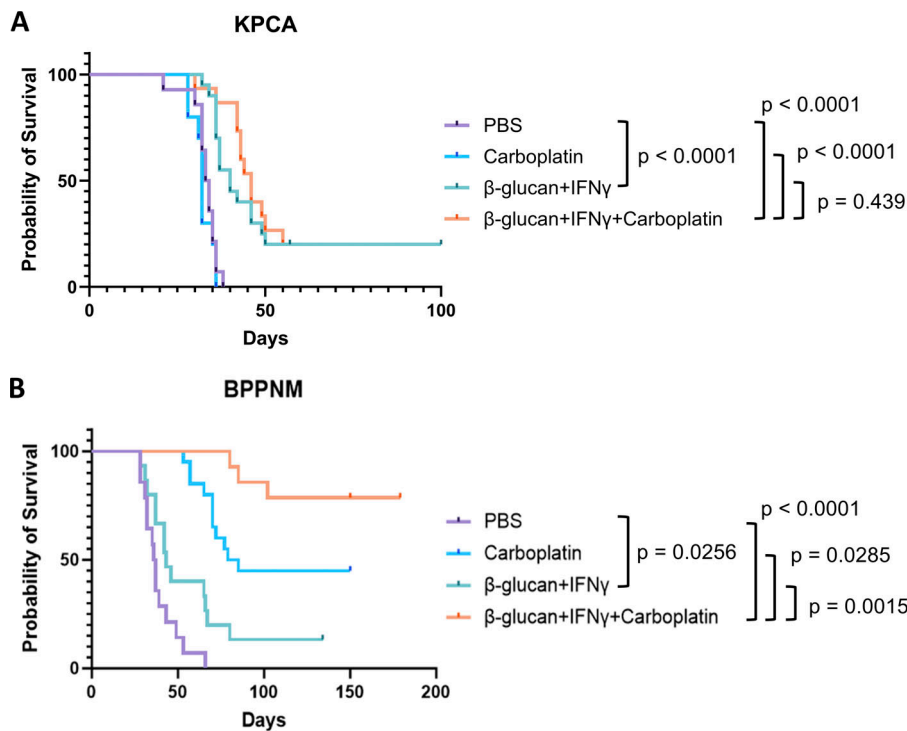


Figure 6. BI extends overall survival in both chemoresistant and chemo-sensitive models and dramatically enhances chemotherapy response in the chemo-sensitive model. (A) Survival curves of KPCA tumor-bearing mice treated with BI and carboplatin as indicated. The number of mice is PBS $n = 14$, carboplatin $n = 10$, BI $n = 20$, BI + carboplatin $n = 15$. The graph is a combination of three independent experiments. (B) Survival curves of BPPNM tumor-bearing mice treated with BI and carboplatin as indicated. The number of mice is PBS $n = 14$, carboplatin $n = 20$, BI $n = 15$, BI + carboplatin $n = 14$. The graph is a combination of three independent experiments. Log-rank test was used.

Discussion

T-cell-based immunotherapy has achieved significant advancements in the treatment of various cancers; however, it has yet to yield effective therapeutic outcomes for metastatic OvCa. In this study, we present an alternative immune therapy which harnesses myeloid cells against aggressive metastatic OvCa. In summary, we report here that β -glucan, a PAMP molecule, in combination with the immunogenic cytokine IFN γ coordinates a robust antitumor response in a patient-relevant murine model of metastatic OvCa. Tumor burden regressed in multiple metastatic compartments including the peritoneal fluid, omentum, and other parts of the peritoneal cavity. Surprisingly, β -glucan alone was sufficient to control fluid tumor burden despite not controlling solid tumor progression. Mechanistically, we demonstrated that sequestration of tumor cells out of the peritoneal fluid requires intraperitoneal clotting accompanied by MDR and Dectin-1-Syk-dependent NETosis in the omentum (Fig. S2 K). Systemic tumor regression following BI was facilitated through tumor-extrinsic signaling, requiring both T cells and IFN γ R signaling from the host. ScrRNA-seq analysis of omentum tumors revealed a selective enrichment of monocyte-derived IL27 $^+$ M Φ s following BI. Neutralizing IL27 in vivo significantly impaired BI-induced antitumor immunity, demonstrating that IL27 indeed drives antitumor immunity likely through M Φ s. In agreement with this notion, M Φ s treated directly with BI in vitro can secrete IL27 and activate CD8 $^+$ T cells in an IL27-dependent manner. Moreover, in patients with metastatic OvCa, IL27/EBI3 co-expression predicted better overall patient survival. Finally, BI significantly extended the overall survival of mice with clinically relevant metastatic OvCa and dramatically enhanced the efficacy of platinum-based chemotherapy in vivo in a clinically relevant, HR-deficient metastatic OvCa model. Taken

together, these data suggest the therapeutic potential of BI in treating metastatic OvCa in patients.

In contrast to the hematological route of metastasis seen in other cancers, OvCa cells readily disseminate directly into the peritoneal fluid as single cells or multicellular aggregates prior to seeding in secondary peritoneal metastatic sites. This route of dissemination is uniquely challenging as these fluid-bound spheroids are functionally dormant, rendering them resistant to anoikis (a form of apoptosis following cell detachment) and proliferation-targeting chemotherapy (Shepherd and Dick, 2022). At the same time, highly invasive and therapy-resistant OvCa stem cells have been reported to be enriched in malignant ascites in patients (Raghavan et al., 2019; Ward Rashidi et al., 2019). One theory of relapse suggests that cancer cells left behind in the fluid following surgical debulking and therapy give rise to chemoresistant patient relapse (Liao et al., 2014; Shepherd and Dick, 2022). Therefore, numerous studies have attempted to elucidate cancer intrinsic vulnerabilities of disseminating cancer cells in the peritoneal fluid in an effort to improve therapy response (Buensuceso et al., 2020; Haagsma et al., 2023; Latifi et al., 2012). To our knowledge, this study is the first of its kind to demonstrate a cancer *extrinsic* approach for targeting these cells. Here we demonstrate that peritoneal immune responses which canonically target pathogens can be exploited to target disseminating cancer cells in the peritoneal fluid, seemingly independently of cell types (Fig. 2 B and Fig. S2 B). Moreover, not only did intraperitoneal β -glucan administration sequester cancer cells out of the peritoneal fluid, it also induced acute cancer killing in peritoneal clots (Fig. S2 G). Interestingly, BI enhanced cancer killing in these clots as well (Fig. S5, H and I). The consequence of clot biology in killing cancer cells remains an open question and warrants further study.

Meanwhile, although the acute fate of cancer cells trapped by the omentum was not investigated in this study, the consequence of rapid sequestration of cancer cells into the omentum still has the potential to revolutionize OvCa treatment. Despite efforts in improving therapeutics against OvCa, one of the greatest predictors of prognosis in stage III and IV patients is still the maximal removal of tumors during cytoreduction surgery (Bristow et al., 2023). Because most OvCa patients will undergo omentectomy as part of treatment, preoperative intraperitoneal administration of β -glucan could potentially improve surgical outcomes by trapping fluid cancer cells in the organ prior to its removal. However, further research is needed to test the efficacy and safety of such an approach. Still, this study shows for the first time that exploring cancer extrinsic mechanisms of cancer targeting in the peritoneal fluid holds promise to address a critical need.

The pleiotropic cytokine IL27 has been reported to contribute to tumor immunity in a context-dependent manner (Fabbi et al., 2017). It was initially reported as an IL12-like cytokine secreted by antigen-presenting cells that drive T-cell activation (Pflanz et al., 2002) and antitumor immunity (Liu et al., 2022; Patidar et al., 2022). More recently, accumulating evidence demonstrates the role of IL27 in promoting expansion of regulatory T cells (Do et al., 2017; Hall et al., 2012), expression of T cell checkpoint receptors (Carbotti et al., 2015; Hirahara et al., 2012), and survival of tumor cells (Jia et al., 2016), revealing its context-dependent role in modulating tumor immunity. This starkly contrasts with IL12, which is universally considered to be anti-tumor. IL12 is strongly induced by PAMP/IFN γ stimulation in vitro and is a hallmark of antitumor M Φ s. Recent in vivo work has demonstrated that co-stimulation of M Φ s by MPLA (a PAMP molecule, acting as a TLR4 agonist) and IFN γ in breast cancer and OvCa induces IL12 production by M Φ s and promotes anti-tumor T cell activity (Sun et al., 2021). However, the serious toxicity of IL12 in humans prevented its clinical usage (Leonard et al., 1997). To this end, IL27 could be a promising cytokine that stimulates local rather than systemic antitumor immunity. Interestingly, in published human and our own mouse scRNA-seq datasets of OvCa, expression of IL12 was not highly induced (Fig. S4, C and F), suggesting that different tumor microenvironments can induce differential antitumor cytokine-secretion in M Φ s. These suggest that IL27 is a promising antitumor cytokine in treating metastatic OvCa. Whether IL27 is a viable therapeutic target in OvCa requires future investigations. Finally, as to the regulation of IL27 expression and secretion, we found that both agents in BI treatment were required to stimulate IL27 heterodimer secretion in vitro. Meanwhile, either β -glucan or IFN γ on their own is sufficient to drive the secretion of IL27p28 (the monomer form is also known as IL30), although BI is still necessary to produce the highest response (Fig. S5 D). This is consistent with previous reports which demonstrated that LPS (another PAMP molecule) induces IL27p28 expression and secretion, and this effect was enhanced by the addition of IFN γ (Liu et al., 2007). Therefore, understanding the genetic regulation of EBI3, the other subunit of IL27, or the secretion of the IL27 heterodimer following BI treatment may ultimately dictate IL27 regulation in M Φ s. Moreover, future studies will answer

how IL27 is induced in vivo and definitively demonstrate its cellular source and target.

To our surprise, we identified two β -glucan-driven mechanisms which did not require canonical Dectin-1-Syk signaling: (1) MDR and MDR-mediated cancer cell capture (Fig. 2, G, K, and L) and (2) IL27 stimulation in M Φ s (Fig. 5 E). This is surprising because Dectin-1 is considered to be the primary receptor for β -glucan signaling in M Φ s (Brown et al., 2002; Goodridge et al., 2011). To our knowledge, while Syk-independent β -glucan signaling has been identified (Gringhuis et al., 2009; Herre et al., 2004), how β -glucan signals in M Φ s independent of Dectin-1 is not well understood. β -glucan can bind to complement and therefore may signal through complement receptor 3 in addition to Dectin-1. However, this interaction has been predominately studied in neutrophils and its contribution to phagocytosis of β -glucan particles in M Φ s (like what is used for this study) is insignificant (Goodridge et al., 2009). Therefore, identifying the mechanism through which β -glucan drives M Φ clotting and IL27 is ongoing.

The ability of the innate immune system to generate memory responses to secondary infectious or inflammatory responses is called immune training (Netea et al., 2016). Immune training can be induced by β -glucan and was initially thought to be only involved in infection and inflammation (Netea et al., 2011; Quintin et al., 2012). Recently, it has been appreciated that β -glucan-mediated immune training could be one approach for the treatment of several cancers, inducing robust antitumor activity and protecting against relapse in preclinical models (Ding et al., 2023; Geller et al., 2022; Kalafati et al., 2020; Woeste et al., 2023). Although we did not set out to comprehensively analyze trained immunity in this study, we did observe an increase in progenitor cell numbers in the bone marrow of mice 1 wk after BI treatment (Fig. S4 B), which may hint at a role of trained immunity for BI efficacy. Conversely, however, we also found that T cells were indispensable for BI-induced antitumor activity against metastatic OvCa. This finding opposes one key hallmark of trained immunity; that is its activity occurs independently of T cells (Kalafati et al., 2020; Priem et al., 2020). Therefore, it is unclear from this study whether immune training contributes to BI antitumor activity. However, future studies are warranted to evaluate this remaining question comprehensively.

In summary, we have established an alternative immune therapy which combines β -glucan and IFN γ to drive regression of metastatic OvCa in vivo. While more work is to be done on elucidating specific antitumor mechanisms in M Φ s and other cell types following β -glucan+IFN γ and its impact on hematopoiesis and immune training, our data suggest (1) a novel concept of targeting tumor cells floating in the fluid by “relocating” them to adherence to an immune-rich environment for better killing and (2) a novel role of IL27 in promoting antitumor immunity in metastatic OvCa. We acknowledge that the antitumor role of IL27⁺ M Φ s is only partially responsible for tumor elimination. Mechanisms mediated by other cell types will be investigated in future studies. Moreover, we propose to further investigate BI because of its tremendous therapeutic potential, which could improve the lives and survival of metastatic OvCa

patients. Finally, while most immunotherapeutic approaches focus on targeting adaptive immunity, our data highlight the importance of harnessing innate immunity in developing robust anti-cancer immunotherapies.

Materials and methods

Cell lines

The original ID8 cell line, derived from spontaneous in vitro malignant transformation of C57BL6 mouse ovarian surface epithelial cells (Roby et al., 2000), was modified to express GFP and firefly luciferase. KPCA, and BPPNM cells, which were recently generated and characterized (Iyer et al., 2021), were generously gifted to us by Drs. Robert Weinberg and David Pepin at the Whitehead Institute, Cambridge, MA, USA, and the Mass General Research Institute, Boston, MA, USA, respectively. KPCA cells were previously modified to express GFP and firefly luciferase. We modified BPPNM cells to express firefly luciferase. All cell lines were cultured in Dulbecco's modified Eagle's medium (10-017-CV; DMEM; Corning) supplemented with 4% FBS (16140-071; Gibco), 1% penicillin/streptomycin, 1X Insulin-Transferrin-Selenium (cat# 41400-045; Gibco), and 2 ng/ml mouse epidermal growth factor at 37°C supplied with 5% CO₂. Cells were passaged no more than five times prior to injection into mouse peritoneal cavities.

Animal models

C57BL/6J (WT, #000664), B6.129S7-*Ifngr*^{tm1Agt/J} (IFN γ RKO, #003288), B6.129S6-Clec7atm1Gdb/J (Dectin-1 KO, # 012337) and B6.Cg-Padi4^{tm1.1Kmo}/J (PAD4 KO, #030315) mice were purchased from Jackson Laboratories. *Lyz2*^{Cre/+}; *Syk*^{fl/fl} (*Syk*^{Mye Δ}) and their Cre negative littermate controls (*Syk*^{WT}) mice were generated by crossing *Lyz2*^{Cre} mice (#004781; Jackson) with *Syk*^{fl/fl} mice, which were generously gifted to us by Dr. John Lukens from the University of Virginia, Charlottesville, VA, USA. All mice were housed in individual microisolator cages in a rack system with filtered air in Wistar's mouse barrier facility and provided with shelter and enrichment to reduce stress. Reducing stress in mice is critical as stress has been reported to impede anti-cancer immunotherapy (Yang et al., 2019). Anecdotally, we observed similar effects in our model. Mice were kept on a 12-h light-dark cycle and had access to food and water ad libitum. All animal procedures were performed in accordance with the Wistar Institutional Animal Care and Use Committee under protocol 201536. Genotyping was performed utilizing Transnetyx automated genotyping services.

Tumor implantation, treatment, and survival

Cells were harvested with trypsin-EDTA (Corning), washed in PBS, and injected i.p. into mice. 3×10^6 ID8 cells were injected in 100 μ l PBS into 8–10-wk-old female WT mice and allowed to seed for 2 wk prior to β -glucan treatment. Mice were treated with 500 μ g sonicated whole β -glucan particles (tlrl-wgp; Invivogen) in PBS i.p. or PBS vehicle control once every other week for 2 wk for a total of two injections (Fig. S1 A). 2 wk after the final dose of β -glucan, tumor burden was assessed by IVIS Spectrum Imaging (PerkinElmer). For KPCA tumors, 1×10^6

KPCA cells were injected i.p. into WT or IFN γ R KO in 200 μ l of a 1:1 matrigel:PBS mix (Matrigel Matrix Basement Membrane, 354234; Corning). Tumors grew for 1 wk prior to treatment. Mice were treated with 500 μ g β -glucan, 20 μ g recombinant mouse IFN γ (315-05; Peprotech), β I, or PBS vehicle control once a week for 2 wk (Fig. S1 B). 1 wk after the final treatment, mice were imaged by IVIS. Importantly, β -glucan was sonicated intermittently on high for 15 min immediately prior to injection to ensure thorough disruption of β -glucan aggregates. Recombinant mouse IFN γ was gently reconstituted in molecular grade, sterile H₂O and diluted in PBS to its working concentration. To preserve IFN γ activity, solutions were handled gently to reduce the presence of bubbles and never vortexed. For macrophage depletion studies, mice were treated with 100 μ l of CLL (C-005; Liposoma) 1 wk prior to cancer capture studies. For tumor studies, 100 μ l of CLL was injected i.p. 5, 9, 14, and 19 days after tumor seeding. On day 14, CLL was administered 4 h before BI treatment. For T cell depletion studies, α CD4 (C2838; Leinco Tech) and α CD8 (C2850; Leinco Tech) monoclonal antibodies were injected 150 μ g each i.p. in WT KPCA tumor-bearing mice 3 days following cancer seeding and then once a week for 2 wk for a total of three injections. For the IL27 neutralization studies, 200 μ g α IL27p28 monoclonal antibody (BE0326; InVivoMAB) (Marillier et al., 2014) was injected 2 days prior to β I treatment, at the same time as treatment, and then two times a week for 2 wk following treatment for a total of six injections. For treatment of experiments with carboplatin, 10–30 mg/kg once a week of carboplatin was administered with or without β I, starting at day 7 for 2 wk. The dose and timing of β -glucan and IFN γ were the same as mentioned above. On day 21, mice were imaged by IVIS and further monitored for survival analysis.

Bioluminescent imaging

In vivo and ex vivo bioluminescence imaging was performed on an IVIS 50 (Living Image 4.3.1; PerkinElmer), with exposures of 1 s to 1 min, binning 2–8, field of view 12.5 cm, f/stop 1, and open filter. For in vivo imaging, D-Luciferin (150 mg/kg in PBS; Gold Biotechnology) was injected into the mice i.p. and imaged 10 min later. Mice were maintained under general anesthesia by continuous inhalation of 2–1.5% isoflurane in 60% oxygen. For ex vivo imaging, mice were injected with D-Luciferin and euthanized after 5 min. Mice peritoneal cavities were exposed, and the omentum was excised. Mouse carcasses (“non-omentum”) and omentum were placed in the machine and imaged as shown in Fig. S2 D. The total photon flux (photons/s) was measured from regions of interest using the Living Image 2.6 program.

Mesentery metastasis scoring

Mesentery metastasis score was calculated based on the following criteria. Whole disseminated mesenteric tumors were counted and each mouse score was determined as follows:

- 0: no tumor was detected,
- 1: number of tumor nodules is <10,
- 2: number of nodules is 10–30,
- 3: number of nodules is over 30.

Acute cancer cell disappearance by β -glucan

2×10^6 cancer cells in 100 μ l of PBS were injected i.p. into 8–12-wk male and female WT, Syk^{Mye Δ} , Syk^{WT}, Dectin-1 KO, or PAD4 KO mice immediately followed by 500 μ g sonicated β -glucan in 100 μ l PBS. 5 h later, mice were euthanized, peritoneal lavage was taken, and the omentum were imaged as described below (Fig. S2 A). Clots were harvested 24 h after β -glucan injection and digested prior to analysis by FACS as described below. Peritoneal lavage and clots were analyzed by FACS for the presence of GFP⁺CD45⁻ cancer cells and F4/80^{hi}ICAM2^{hi}CD11b^{high} PRM Φ s. Omentum was imaged to identify the presence of GFP⁺ cancer cells. To reduce background fluorescence, the omentum was gently stretched over the liver and imaged. For mice treated with heparin, 100 U/mouse of heparin was given in the same syringe as β -glucan. In the M Φ depletion model, mice were treated with 100 μ l of CLL 1 wk prior to cancer cell capture assays. Omentectomized mice were allowed to recover for 4 wk prior to entering this study. Data from combined experiments are presented as fold change. Fold change was calculated as $n \div \text{avg of the control}$ where n = experimental value.

Omentectomy

Extended-release buprenorphine (3.25 mg/kg) was given subcutaneously preoperatively for pain management. Surgical removal of the omentum was accomplished under general anesthesia by continuous inhalation of 2–3% isoflurane in 60% oxygen using a veterinary vaporizer. Aseptic techniques were performed to maintain sterility in the surgical field. 6–8-wk-old male and female mice were used. Mice were placed on a heating pad in a supine position. A midline incision was made in the region of the stomach and the greater omentum was carefully exposed. The omentum is a thin, elongated adipose tissue that is located under the stomach and between the spleen and pancreas. The omentum was removed via electrocautery to avoid bleeding and the midline incision was closed with absorbable sutures in two layers (first the peritoneal wall was closed and then the skin). Mice were immediately placed in a clean heated cage and monitored until awake. A liquid recovery diet was provided, and mice were monitored daily for 7 days for signs of infection. Removal of both the entire greater and lesser omentum results in malperfusion of the stomach and spleen and thus was not feasible. Mice were allowed to recover for 4 wk before any further experimental procedures were performed.

Collection of peritoneal lavage and tissue dissociation

Peritoneal lavage was collected by flushing the peritoneal cavity with 6 ml FACS buffer (PBS with 2 mM EDTA and 0.1% BSA). Mice were gently massaged to ensure optimal collection of peritoneal cells. Peritoneal clots were collected 24 h after β -glucan injection and omentum tumors were collected at the conclusion of each study. Clots and tumors were digested in the same way using a cocktail of 1 mg/ml collagenase IV and 100 μ g/ml DNase I, in 1–4 ml DMEM with 10% FBS depending on tissue size. The tissues were minced into small pieces prior to digestion at 37°C for 30 min shaking at 800 rpm. Samples were then passed through a 70 μ m cell strainer to collect single-cell suspension to be analyzed by flow cytometry. If necessary, single-

cell suspensions were treated with 1X red blood cell lysis buffer (555899; BD Bioscience) on ice for 10 min.

Flow cytometry

Single-cell suspensions were collected as described above prior to staining with primary conjugated antibodies at their indicated dilutions (Table S1). Surface stain antibodies were incubated with cells on ice for 30 min and washed with 1 ml FACS buffer (PBS with 2 mM EDTA and 0.1% BSA). Intracellular staining was carried out using True-Nuclear Transcription Factor Buffer Set (424401; Biolegend) according to manufacturer instructions. Briefly, cells were fixed for 45 min–1 h at room temperature in the dark. Notably, KPCA cells lose GFP signal following fixation. Following fixation, cells were washed 1 \times in permeabilization buffer and then incubated in permeabilization buffer with intracellular stain antibodies overnight at 4°C. Counting beads (424902; Biolegend) were added to each sample to determine cell numbers. Samples were analyzed on a BD FACSymphony A3 Cell Analyzer using FlowJo software. For IFN γ and TNF staining in T cells, single cells from the omentum tumor were incubated for 4 h with Cell Activation Cocktail (with Brefeldin A) (catalog no. 423303; Biolegend) prior to staining.

To analyze bone marrow progenitors, $2\text{--}5 \times 10^6$ bone marrow cells were stained as single cells suspension in FACS buffer for 100 min at 4°C as follows. Cells were incubated with Aqua Live/Dead (BV510) and anti-CD16/32 BV711. After 10 min, the anti-CD34 PE was added. After 30 min, the remaining antibodies cocktail was added (anti-LY6G BUV563, B220 FITC, CD90.2 FITC, NK1.1 BUV661, Sca1 PerCpCy5.5, CD117 [cKit] BV786, CD135 BV4221, CD150 PECy5, CD48 AF700, LY6C BV605, CD81 PECy7, CD115 PE/Dazzle, CD11B BUV805, CD106 BUV737). Cells were washed and resuspended in 500 μ l of FACS Buffer and acquired with a BD FACSymphony A5 Cell Analyzer and analyzed using FlowJo software.

Fluorescence imaging

5 h after the injection of β -glucan and KPCA cells, the omentum was excised and fixed in 4% paraformaldehyde overnight at 4°C. On the next day, the tissues were rinsed with 3 \times PBS, blocked with 3% BSA and 1% Triton in PBS at room temperature for 60 min, and incubated with primary antibodies at their optimized dilutions (Table S1)— α -CHH3 and α -S100A9 overnight at 4°C. The tissues were then washed with 3 \times PBS before being incubated with respective secondary antibodies at room temperature for 1 h. After washing, the tissues were stored in PBS. Whole-mount confocal images were collected using a Leica SP8 microscope.

In situ omentum images were also taken using a Leica M205 FA fluorescence stereo microscope. Briefly, shortly following euthanization, the mice peritoneal cavities were exposed, and the omentum was located. Because several organs autofluoresce, such as the intestines (Fig. S2 D), the omentum was gently stretched over the liver, which does not autofluoresce, prior to imaging to minimize background.

Quantitative RT-PCR (qRT-PCR)

The femur and tibia were harvested from 8-wk-old C57BL6 mouse. Two ends of the bones were cut and the bone marrow was flushed with a 26 g needle filled with cold sterile 1X PBS

through a 40 μm cell strainer. 10 ml total PBS was used for all four bones. The bone marrow was centrifuged at 500 g for 5 min at 4°C and then the pellet was resuspended in 500 μl of FACS buffer.

Monocytes were isolated using EasySep Mouse Monocyte Isolation Kit (#19861; Stem Cell Technologies) and plated at a density of 200,000 cells per well of a 24-well plate (4×10^5 cells/ml). Monocytes were differentiated in the presence of 20 ng/ml of CSF1 in RPMI with 10% FBS and 1x penicillin/streptomycin. After 24 h in culture, 10 $\mu\text{g}/\text{ml}$ β -glucan and 33 ng/ml IFN γ were added for an additional 48 h. Total RNA was isolated from cultured cells using TRIzolTM reagent (Invitrogen), according to the manufacturer's protocols. Glycoblue (Invitrogen) was added as a co-precipitant when handling $<10^6$ cells.

cDNA was synthesized using a High-Capacity RNA-to-cDNA Kit (#4387406; Applied Biosystems), according to the manufacturer's protocols. qRT-PCR was performed using SYBR Green PCR Master Mix (#4344463; Applied Biosystems) on a QuantStudio 3 Real-Time PCR Instrument (Applied Biosystems). The following primers were used for qRT-PCR:

Vcam1 forward primer 5'-AGTTGGGGATTCCGGTTGTTCT-3'; Vcam1 reverse primer 5'-CCCCTCATTCTTACCACCC-3'; C1qa forward primer 5'-AAAGGCAATCCAGGCAATATCA-3'; C1qa reverse primer 5'-TGTTCTGGTATGGACTCTCC-3'; H2-eb1 forward primer 5'-GCCGAGAGTTGAGCCTACG-3'; H2-eb1 reverse primer 5'-CCAGGAGTTGTTGGTGTTC-3'; Ccl8 forward primer 5'-TCTACGCAGTGCTTCTTTGCC-3'; Ccl8 reverse primer 5'-AAGGGGATCTTCAGCTTTAGTA-3'; Il27 forward primer 5'-CTGTTGCTGCTACCCTTGCTT-3'; Il27 reverse primer 5'-CAC TCCTGGCAATCGAGA-3'; Gapdh forward primer 5'-AGGTCG GTGTGAACGGATTTG-3'; Gapdh reverse primer 5'-TGTAGA CCATGTAGTTGAGGTCA-3'.

All data were normalized to Gapdh quantified in parallel amplification reactions.

Single-cell sequencing and analysis of mouse tumors

Prior to sequencing, immune cells (minus B cells, CD45⁺CD19⁻) were sorted from omentum tumor samples (three mice/group) and pooled. Samples were uniquely barcoded using TotalSeq-B mouse hashtag antibodies (BioLegend), as per the manufacturer's directions, to allow for sample multiplexing for the 10x Genomics Chromium Controller single-cell platform (10x Genomics). Specifically, 1–2 million cells of each sample were first blocked with TruStain FcX PLUS anti-mouse CD16/32 antibody and then incubated with 0.5 μg of various anti-mouse hashtag antibodies carrying unique cell barcodes. One 10x G chip lane was loaded with a pool of four uniquely barcoded samples and single-cell droplets were generated using the Chromium Next GEM single cell 3' kit v3.1 (10x Genomics). cDNA synthesis and amplification, library preparation, and indexing were done using the 10x Genomics Library Preparation kit (10x Genomics), according to the manufacturer's instructions. Overall library size was determined using the Agilent Bioanalyzer 2100 and the High Sensitivity DNA assay and libraries were quantitated using KAPA real-time PCR. One library consisting of a total of four samples was pooled and sequenced on the NextSeq 2000 (Illumina) using a P3

100 cycle kit (Illumina), paired end run with the following run parameters: 28 base pair \times 8 base pair (index) \times 90 base pair.

Pre-processing of the scRNA-seq data was performed using Cell Ranger Suite (pipeline v7.0.0, <https://support.10xgenomics.com>) with refdata-gex-mm10-2020-A transcriptome as a reference to map reads on the mouse genome (mm10) using STAR (Dobin et al., 2013). Cells with over 5% mitochondrial content were filtered out as were those with <200 genes with reads to remove cells with low quality and/or cells that are likely dying. The remaining 13534 cells were used for downstream analysis. Batch effect was not observed and hence not corrected for. Seurat v4 (Hao et al., 2021) was used for cell clustering, marker identification, and visualization. The R package SingleR (Aran et al., 2019) was used to determine the initial cell types of the clusters using the MouseRNASeq dataset as a reference for cell-specific gene signatures and then verified using known cell-type markers unique to clusters. The M Φ /monocyte clusters were subset and reclustered to identify subclusters of interest. The R package Slingshot (Street et al., 2018) was used for trajectory analysis of the M Φ /monocyte subclusters. Differential expression between samples in specific clusters was performed using the Wilcoxon Rank Sum Test. Statistically significant differentially expressed genes were used as inputs for enrichment analysis using Qiagen IPA. Raw data have been deposited onto Gene Expression Omnibus (GSE278380).

scRNA-seq analysis of human OvCa samples

We obtained a scRNA-seq dataset deposited by Vázquez-García et al. from the National Center for Biotechnology Information Gene Expression Omnibus (GSE180661) (Vázquez-García et al., 2022). The dataset consisted of quality-filtered matrices of 929,686 cells. The Seurat package v4.3.0 (RRID:SCR_016341) in R software v4.3.1 (RRID:SCR_001905) and the scanpy package v1f.9.3 (RRID:SCR_018139) in Python 3.10 (RRID:SCR_008394) were used for downstream processing. Dimensionality reduction was performed using principal component analysis and uniform manifold approximation and projection (UMAP), the same protocol as in the original article. We used the cell type annotation assigned in the original article. The R package scCustomize v1.1.1 and the scanpy function score_genes were used to generate joint plots.

Kaplan Meier (KM) plotter

The KM Plotter Online tool (<https://kmplot.com/analysis/>) (Györfy, 2024) was used to evaluate the relationship between high gene expression and clinical outcomes in patients with late-stage OvCa (stages III and IV). This open-access The Cancer Genome Atlas-based database contains bulk RNA sequencing datasets from 1,268 late-stage OvCa patients, which allowed us to investigate the correlation between overall survival and enriched genes identified by our scRNA-seq analysis in patients. To analyze the correlation between IL27/EBI3 co-expression and overall survival, we utilized the multiple-gene analysis and assigned equal weights to IL27 and EBI3.

In vitro IL27 induction

The femur and tibia were harvested from 8-wk-old C57BL6, *Syk^{MyeΔ}*, *Dectin-1 KO*, or *IFN γ R-KO* mouse. Two ends of the bones were cut, and the bone marrow was flushed with a 26 g needle filled with cold sterile 1X PBS through a 40- μ m cell strainer. 10 ml total PBS was used for all four bones. BMDMs were differentiated from total bone marrow cells by growing them in the presence of 20 ng/ml of CSF1 in RPMI with 10% FBS and 1x penicillin/streptomycin. Media was supplemented with 0.5 the volume of initial media+CSF1 and differentiation was complete by day 6. After differentiation, the media was changed and BMDMs were stimulated with 10 μ g/ml β -glucan and 33 ng/ml IFN γ for 24–48-h. IL27 heterodimer and IL27p28 ELISAs were performed according to their manufacturer protocols (438707; Biolegend, and M2728; R&D Biotechne, respectively).

T cell activation assay

For T cell activation assay, we treated BMDM with 10 μ g/ml β -glucan and 33 ng/ml IFN γ for 24 h. OT-I T cells (CD8⁺) were isolated from spleens of OT-I mice using EasySep Mouse CD8⁺ T Cell Isolation Kit (19853A; Stem Cell Technologies). DCs were isolated from spleens of WT mice using EasySep Mouse Pan-DC Enrichment Kit II (19863; Stem Cell Technologies). Co-cultures were set up in four replicates with BMDM primed as above, OT-I T cells, and DCs in the presence of OVA257-264 peptide (AS-60193-1; Ana Spec, Inc.) at 0.5 ng/ml for 3 days. DCs were added at a 1:10 ratio to T cells.

For staining surface markers, cells were incubated with a fluorescent-conjugated antibody cocktail for staining at 4°C for 30 min. For intracellular staining, cells were stimulated with 20 ng/ml of PMA, 1 μ g/ml of ionomycin, 3 μ g/ml of brefeldin A, and 2 μ M of monensin and incubated at 37°C for 4 h. Cells were incubated with an antibody cocktail for surface markers at 4°C for 30 min and then fixed using a True nuclear transcription factor buffer set (Cat # 424401; Biolegend) for 20 min at 4°C. Cell pellets were incubated with an antibody cocktail for intracellular markers prepared in permeabilization buffer and incubated at 4°C for 30 min. All the antibodies were used at 1:400 dilution. Samples were then washed and resuspended in 1x PBS and acquired on BD FACS Symphony flow cytometer. Data were analyzed using FlowJo v10 (Treestar, Inc.).

Statistics

Statistical analyses were performed in Prism (GraphPad Software, Inc.). Statistical tests used and other relevant details are noted in the figure legends. Statistical analysis was performed using the Student's *t* test for unpaired samples or one-way ANOVA with a post-hoc Tukey's multiple comparisons test. Results were considered significant at $P < 0.05$. Results display all replicated experiments and are presented as mean \pm SEM.

Illustration

Graphical abstract and Fig. S2 K were generated using <https://Biorender.com>.

Online supplemental material

Fig. S1 illustrates in vivo treatment regimens, staging of tumor pathology at time of treatment and clearance of ascites following

β -glucan treatment. Fig. S2 provides additional support for β -glucan-mediated cancer capture including ID8 capture and clodronate-loaded liposome macrophage depletion experiments. Fig. S2 also provides an illustration describing the cancer capture mechanism discovered in this study. Fig. S3 includes additional tumor burden evaluations following BI treatment as well as an IDEXX analysis of BI toxicity. Fig. S4 analyzes M Φ subpopulations and progenitor cells following BI treatment. Fig. S4 also includes immune cell population clustering of human scRNA-seq data and expression of *IL12A* and *IL12B* in myeloid subclusters from human OvCa tumors. Fig. S5 shows expression of TNF and IFN γ in CD4⁺ and CD8⁺ T cells following BI treatment with and without IL27 neutralization. Additionally, Fig. S5 shows TUNEL staining quantification in clots from BI-treated mice. Finally, Table S1 lists information for all antibodies used in this study.

Data availability

The human sequencing data in Fig. 4 and Fig. S4 are openly available in the Gene Expression Omnibus (GSE278380). Remaining data are available from the corresponding author upon reasonable request. All the data needed to evaluate the conclusions of the paper are present in the paper or the online supplemental material.

Acknowledgments

We thank Wistar core facilities (imaging, histology, flow cytometry, animal facility, and genomics). We thank Drs. Chris Hunter and Li-Fan Lu for discussions on IL27 and Dr. Maureen Murphy for proofreading the manuscript.

This study was supported by National Institutes of Health (NIH) Career Enhancement Program through Hopkins-Penn-Wistar Ovarian Cancer Specialized Ovarian Cancer Research (P50CA228991; N. Zhang), Department of Defense Ovarian Cancer Research Program (HT94252410206; N. Zhang), W.W. Smith Charitable Trust (C2205; N. Zhang), National Institute of Allergy and Infectious Diseases (NIAID) (K99AI151198; N. Zhang), National Institute of Neurological Disorders and Stroke (1R01NS131912; F. Veglia), National Cancer Institute (NCI) (1R37CA280869; R. Shinde), NCI (1R21CA259240; R. Shinde), NIAID (5R21AI175738; L. Huang), Cancer Center Support Grant (P30CA010815; N. Zhang), NIH Wistar Training Program in Basic Cancer Research (T32 CA009171; B. Murphy), and Japan Society for the Promotion of Science (202360517; T. Miyamoto).

Author contributions: B. Murphy: Conceptualization, Data curation, Formal analysis, Investigation, Methodology, Visualization, Writing - original draft, Writing - review & editing, T. Miyamoto: Conceptualization, Investigation, Methodology, Validation, Writing - original draft, Writing - review & editing, B.S. Manning: Formal analysis, Investigation, Visualization, G. Mirji: Formal analysis, Investigation, Visualization, Writing - review & editing, A. Ugolini: Investigation, T. Kannan: Data curation, Formal analysis, Visualization, K. Hamada: Data curation, Formal analysis, Writing - review & editing, Y.P. Zhu: Validation, D.T. Claiborne: Data curation, Resources, Supervision, Writing - review & editing, L. Huang: Writing - review & editing, R.

Zhang: Resources, Supervision, Writing - review & editing, Y. Nefedova: Resources, Writing - review & editing, A. Kossenkov: Data curation, Formal analysis, Software, Validation, Visualization, Writing - review & editing, F. Veglia: Investigation, Writing - review & editing, R. Shinde: Conceptualization, Data curation, Formal analysis, Investigation, Methodology, Resources, Supervision, Validation, N. Zhang: Conceptualization, Data curation, Formal analysis, Funding acquisition, Investigation, Methodology, Project administration, Supervision, Validation, Visualization, Writing - original draft, Writing - review & editing.

Disclosures: Y. Nefedova reported grants from Buzzard Pharmaceuticals, grants from Active Biotech, and grants from Jubilant Therapeutics, Inc. outside the submitted work. No other disclosures were reported.

Submitted: 26 October 2023

Revised: 14 June 2024

Accepted: 15 October 2024

References

- Almeida-Nunes, D.L., A. Mendes-Frias, R. Silvestre, R.J. Dinis-Oliveira, and S. Ricardo. 2022. Immune tumor microenvironment in ovarian cancer ascites. *Int. J. Mol. Sci.* 23:10692. <https://doi.org/10.3390/ijms231810692>
- Alspach, E., D.M. Lussier, and R.D. Schreiber. 2019. Interferon γ and its important roles in promoting and inhibiting spontaneous and therapeutic cancer immunity. *Cold Spring Harb. Perspect. Biol.* 11:a028480. <https://doi.org/10.1101/cshperspect.a028480>
- Aran, D., A.P. Looney, L. Liu, E. Wu, V. Fong, A. Hsu, S. Chak, R.P. Naikawadi, P.J. Wolters, A.R. Abate, et al. 2019. Reference-based analysis of lung single-cell sequencing reveals a transitional profibrotic macrophage. *Nat. Immunol.* 20:163–172. <https://doi.org/10.1038/s41590-018-0276-y>
- Barth, M.W., J.A. Hendrzak, M.J. Melnickoff, and P.S. Morahan. 1995. Review of the macrophage disappearance reaction. *J. Leukoc. Biol.* 57:361–367. <https://doi.org/10.1002/jlb.57.3.361>
- Bradner, W.T., D.A. Clarke, and C.C. Stock. 1958. Stimulation of host defense against experimental cancer. I. Zymosan and sarcoma 180 in mice. *Cancer Res.* 18:347–351.
- Bristow, R.E., R.S. Tomacruz, D.K. Armstrong, E.L. Trimble, and F.J. Montz. 2023. Survival effect of maximal cytoreductive surgery for advanced ovarian carcinoma during the platinum era: A meta-analysis. *J. Clin. Oncol.* 41:4065–4076. <https://doi.org/10.1200/JCO.22.02765>
- Brown, G.D., P.R. Taylor, D.M. Reid, J.A. Willment, D.L. Williams, L. Martinez-Pomares, S.Y. Wong, and S. Gordon. 2002. Dectin-1 is a major beta-glucan receptor on macrophages. *J. Exp. Med.* 196:407–412. <https://doi.org/10.1084/jem.20020470>
- Buensuceso, A., Y. Ramos-Valdes, G.E. DiMattia, and T.G. Shepherd. 2020. AMPK-independent LKB1 activity is required for efficient epithelial ovarian cancer metastasis. *Mol. Cancer Res.* 18:488–500. <https://doi.org/10.1158/1541-7786.MCR-19-0530>
- Carbotti, G., G. Barisione, I. Airolidi, D. Mezzanzanica, M. Bagnoli, S. Ferrero, A. Petretto, M. Fabbri, and S. Ferrini. 2015. IL-27 induces the expression of IDO and PD-L1 in human cancer cells. *Oncotarget.* 6:43267–43280. <https://doi.org/10.18632/oncotarget.6530>
- Casanova-Acebes, M., M.P. Menéndez-Gutiérrez, J. Porcuna, D. Álvarez-Erriero, Y. Lavin, A. García, S. Kobayashi, J. Le Berichel, V. Núñez, F. Were, et al. 2020. RXRs control serous macrophage neonatal expansion and identity and contribute to ovarian cancer progression. *Nat. Commun.* 11:1655. <https://doi.org/10.1038/s41467-020-15371-0>
- Català, C., M. Velasco-de Andrés, S. Casadó-Llombart, A. Leyton-Pereira, L. Carrillo-Serradell, M. Isamat, and F. Lozano. 2022. Innate immune response to peritoneal bacterial infection. *Int. Rev. Cell Mol. Biol.* 371:43–61. <https://doi.org/10.1016/bs.ircmb.2022.04.014>
- Celada, A., P.W. Gray, E. Rinderknecht, and R.D. Schreiber. 1984. Evidence for a gamma-interferon receptor that regulates macrophage tumoricidal activity. *J. Exp. Med.* 160:55–74. <https://doi.org/10.1084/jem.160.1.55>
- Chan, S.H., B. Perussia, J.W. Gupta, M. Kobayashi, M. Pospisil, H.A. Young, S.F. Wolf, D. Young, S.C. Clark, and G. Trinchieri. 1991. Induction of interferon gamma production by natural killer cell stimulatory factor: Characterization of the responder cells and synergy with other inducers. *J. Exp. Med.* 173:869–879. <https://doi.org/10.1084/jem.173.4.869>
- Charoentong, P., F. Finotello, M. Angelova, C. Mayer, M. Efremova, D. Rieder, H. Hackl, and Z. Trajanoski. 2017. Pan-cancer immunogenomic analyses reveal genotype-immunophenotype relationships and predictors of response to checkpoint blockade. *Cell Rep.* 18:248–262. <https://doi.org/10.1016/j.celrep.2016.12.019>
- Cheung, N.K., S. Modak, A. Vickers, and B. Knuckles. 2002. Orally administered beta-glucans enhance anti-tumor effects of monoclonal antibodies. *Cancer Immunol. Immunother.* 51:557–564. <https://doi.org/10.1007/s00262-002-0321-3>
- Colombo, N., D. Lorusso, and P. Scollo. 2017. Impact of recurrence of ovarian cancer on quality of life and outlook for the future. *Int. J. Gynecol. Cancer.* 27:1134–1140. <https://doi.org/10.1097/IGC.0000000000001023>
- Ding, C., R. Shrestha, X. Zhu, A.E. Geller, S. Wu, M.R. Woeste, W. Li, H. Wang, F. Yuan, R. Xu, et al. 2023. Inducing trained immunity in pro-metastatic macrophages to control tumor metastasis. *Nat. Immunol.* 24:239–254. <https://doi.org/10.1038/s41590-022-01388-8>
- Do, J., D. Kim, S. Kim, A. Valentin-Torres, N. Dvorina, E. Jang, V. Nagarajavel, T.M. DeSilva, X. Li, A.H. Ting, et al. 2017. Treg-specific IL-27Ra deletion uncovers a key role for IL-27 in Treg function to control autoimmunity. *Proc. Natl. Acad. Sci. USA.* 114:10190–10195. <https://doi.org/10.1073/pnas.1703100114>
- Dobin, A., C.A. Davis, F. Schlesinger, J. Drenkow, C. Zaleski, S. Jha, P. Batut, M. Chaisson, and T.R. Gingeras. 2013. STAR: Ultrafast universal RNA-seq aligner. *Bioinformatics.* 29:15–21. <https://doi.org/10.1093/bioinformatics/bts635>
- Etzerodt, A., M. Moulin, T.K. Doktor, M. Delfini, N. Mossadegh-Keller, M. Bajenoff, M.H. Sieweke, S.K. Moestrup, N. Auphan-Anezin, and T. Lawrence. 2020. Tissue-resident macrophages in omentum promote metastatic spread of ovarian cancer. *J. Exp. Med.* 217:e20191869. <https://doi.org/10.1084/jem.20191869>
- Fabbri, M., G. Carbotti, and S. Ferrini. 2017. Dual roles of IL-27 in cancer biology and immunotherapy. *Mediators Inflamm.* 2017:3958069. <https://doi.org/10.1155/2017/3958069>
- Geller, A.E., R. Shrestha, M.R. Woeste, H. Guo, X. Hu, C. Ding, K. Andreeva, J.H. Chariker, M. Zhou, D. Tieri, et al. 2022. The induction of peripheral trained immunity in the pancreas incites anti-tumor activity to control pancreatic cancer progression. *Nat. Commun.* 13:759. <https://doi.org/10.1038/s41467-022-28407-4>
- Goodridge, H.S., C.N. Reyes, C.A. Becker, T.R. Katsumoto, J. Ma, A.J. Wolf, N. Bose, A.S. Chan, A.S. Magee, M.E. Danielson, et al. 2011. Activation of the innate immune receptor Dectin-1 upon formation of a ‘phagocytic synapse’. *Nature.* 472:471–475. <https://doi.org/10.1038/nature10071>
- Goodridge, H.S., A.J. Wolf, and D.M. Underhill. 2009. Beta-glucan recognition by the innate immune system. *Immunol. Rev.* 230:38–50. <https://doi.org/10.1111/j.1600-065X.2009.00793.x>
- Gringhuis, S.I., J. den Dunnen, M. Litjens, M. van der Vlist, B. Wevers, S.C. Bruijns, and T.B. Geijtenbeek. 2009. Dectin-1 directs T helper cell differentiation by controlling noncanonical NF-kappaB activation through Raf-1 and Syk. *Nat. Immunol.* 10:203–213. <https://doi.org/10.1038/ni.1692>
- Györfy, B. 2024. Transcriptome-level discovery of survival-associated biomarkers and therapy targets in non-small-cell lung cancer. *Br. J. Pharmacol.* 181:362–374. <https://doi.org/10.1111/bph.16257>
- Haagsma, J., B. Kolendowski, A. Buensuceso, Y.R. Valdes, G.E. DiMattia, and T.G. Shepherd. 2023. Gain-of-function p53^{R175H} blocks apoptosis in a precursor model of ovarian high-grade serous carcinoma. *Sci. Rep.* 13:11424. <https://doi.org/10.1038/s41598-023-38609-5>
- Hall, A.O., D.P. Beiting, C. Tato, B. John, G. Oldenhove, C.G. Lombana, G.H. Pritchard, J.S. Silver, N. Bouladoux, J.S. Stumhofer, et al. 2012. The cytokines interleukin 27 and interferon- γ promote distinct Treg cell populations required to limit infection-induced pathology. *Immunity.* 37:511–523. <https://doi.org/10.1016/j.immuni.2012.06.014>
- Hao, Y., S. Hao, E. Andersen-Nissen, W.M. Mauck III, S. Zheng, A. Butler, M.J. Lee, A.J. Wilk, C. Darby, M. Zager, et al. 2021. Integrated analysis of multimodal single-cell data. *Cell.* 184:3573–3587.e29. <https://doi.org/10.1016/j.cell.2021.04.048>
- Herre, J., A.S. Marshall, E. Caron, A.D. Edwards, D.L. Williams, E. Schweighoffer, V. Tybulewicz, C. Reis e Sousa, S. Gordon, and G.D. Brown. 2004. Dectin-1 uses novel mechanisms for yeast phagocytosis in macrophages. *Blood.* 104:4038–4045. <https://doi.org/10.1182/blood-2004-03-1140>

- Hirahara, K., K. Ghoreschi, X.P. Yang, H. Takahashi, A. Laurence, G. Vahedi, G. Sciumè, A.O. Hall, C.D. Dupont, L.M. Francisco, et al. 2012. Interleukin-27 priming of T cells controls IL-17 production in trans via induction of the ligand PD-L1. *Immunity*. 36:1017–1030. <https://doi.org/10.1016/j.immuni.2012.03.024>
- Hong, F., J. Yan, J.T. Baran, D.J. Allendorf, R.D. Hansen, G.R. Ostroff, P.X. Xing, N.K. Cheung, and G.D. Ross. 2004. Mechanism by which orally administered beta-1,3-glucans enhance the tumoricidal activity of anti-tumor monoclonal antibodies in murine tumor models. *J. Immunol.* 173:797–806. <https://doi.org/10.4049/jimmunol.173.2.797>
- Iyer, S., S. Zhang, S. Yucler, H. Horn, S.G. Smith, F. Reinhardt, E. Hoefsmitt, B. Assatova, J. Casado, M.C. Meinsohn, et al. 2021. Genetically defined syngeneic mouse models of ovarian cancer as tools for the discovery of combination immunotherapy. *Cancer Discov.* 11:384–407. <https://doi.org/10.1158/2159-8290.CD-20-0818>
- Izar, B., I. Tirosch, E.H. Stover, I. Wakiro, M.S. Cuoco, I. Alter, C. Rodman, R. Leeson, M.J. Su, P. Shah, et al. 2020. A single-cell landscape of high-grade serous ovarian cancer. *Nat. Med.* 26:1271–1279. <https://doi.org/10.1038/s41591-020-0926-0>
- Jackson-Jones, L.H., P. Smith, J.R. Portman, M.S. Magalhaes, K.J. Mylonas, M.M. Vermeren, M. Nixon, B.E.P. Henderson, R. Dobie, S. Vermeren, et al. 2020. Stromal cells covering omental fat-associated lymphoid clusters trigger formation of neutrophil aggregates to capture peritoneal contaminants. *Immunity*. 52:700–715.e6. <https://doi.org/10.1016/j.immuni.2020.03.011>
- Jia, H., P. Dilger, C. Bird, and M. Wadhwa. 2016. IL-27 promotes proliferation of human leukemic cell lines through the MAPK/ERK signaling pathway and suppresses sensitivity to chemotherapeutic drugs. *J. Interferon Cytokine Res.* 36:302–316. <https://doi.org/10.1089/jir.2015.0091>
- Kaczanowska, S., D.W. Beury, V. Gopalan, A.K. Tycko, H. Qin, M.E. Clements, J. Drake, C. Nwanze, M. Murgai, Z. Rae, et al. 2021. Genetically engineered myeloid cells rebalance the core immune suppression program in metastasis. *Cell*. 184:2033–2052.e21. <https://doi.org/10.1016/j.cell.2021.02.048>
- Kalafati, L., I. Kourtzelis, J. Schulte-Schrepping, X. Li, A. Hatzioannou, T. Grinenko, E. Hagag, A. Sinha, C. Has, S. Dietz, et al. 2020. Innate immune training of granulopoiesis promotes anti-tumor activity. *Cell*. 183:771–785.e12. <https://doi.org/10.1016/j.cell.2020.09.058>
- Krishnan, V., S. Tallapragada, B. Schaar, K. Kamat, A.M. Chanana, Y. Zhang, S. Patel, V. Parkash, C. Rinker-Schaeffer, A.K. Folkins, et al. 2020. Omental macrophages secrete chemokine ligands that promote ovarian cancer colonization of the omentum via CCR1. *Commun. Biol.* 3:524. <https://doi.org/10.1038/s42003-020-01246-z>
- Latifi, A., R.B. Luwor, M. Bilandzic, S. Nazaretian, K. Stenvers, J. Pyman, H. Zhu, E.W. Thompson, M.A. Quinn, J.K. Findlay, and N. Ahmed. 2012. Isolation and characterization of tumor cells from the ascites of ovarian cancer patients: Molecular phenotype of chemoresistant ovarian tumors. *PLoS One*. 7:e46858. <https://doi.org/10.1371/journal.pone.0046858>
- Lee, W., S.Y. Ko, M.S. Mohamed, H.A. Kenny, E. Lengyel, and H. Naora. 2019. Neutrophils facilitate ovarian cancer premetastatic niche formation in the omentum. *J. Exp. Med.* 216:176–194. <https://doi.org/10.1084/jem.20181170>
- Lengyel, E. 2010. Ovarian cancer development and metastasis. *Am. J. Pathol.* 177:1053–1064. <https://doi.org/10.2353/ajpath.2010.100105>
- Leonard, J.P., M.L. Sherman, G.L. Fisher, L.J. Buchanan, G. Larsen, M.B. Atkins, J.A. Sosman, J.P. Dutcher, N.J. Vogelzang, and J.L. Ryan. 1997. Effects of single-dose interleukin-12 exposure on interleukin-12-associated toxicity and interferon-gamma production. *Blood*. 90:2541–2548.
- Li, P., M. Li, M.R. Lindberg, M.J. Kennett, N. Xiong, and Y. Wang. 2010. PAD4 is essential for antibacterial innate immunity mediated by neutrophil extracellular traps. *J. Exp. Med.* 207:1853–1862. <https://doi.org/10.1084/jem.20100239>
- Liao, J., F. Qian, N. Tchabo, P. Mhawech-Fauceglia, A. Beck, Z. Qian, X. Wang, W.J. Huss, S.B. Lele, C.D. Morrison, and K. Odunsi. 2014. Ovarian cancer spheroid cells with stem cell-like properties contribute to tumor generation, metastasis and chemotherapy resistance through hypoxia-resistant metabolism. *PLoS One*. 9:e84941. <https://doi.org/10.1371/journal.pone.0084941>
- Liu, J., X. Guan, and X. Ma. 2007. Regulation of IL-27 p28 gene expression in macrophages through MyD88- and interferon-gamma-mediated pathways. *J. Exp. Med.* 204:141–152. <https://doi.org/10.1084/jem.20061440>
- Liu, J.Q., C. Zhang, X. Zhang, J. Yan, C. Zeng, F. Talebian, K. Lynch, W. Zhao, X. Hou, S. Du, et al. 2022. Intratumoral delivery of IL-12 and IL-27 mRNA using lipid nanoparticles for cancer immunotherapy. *J. Control Release*. 345:306–313. <https://doi.org/10.1016/j.jconrel.2022.03.021>
- Long, L., Y. Hu, T. Long, X. Lu, Y. Tuo, Y. Li, and Z. Ke. 2021. Tumor-associated macrophages induced spheroid formation by CCL18-ZEB1-M-CSF feedback loop to promote transcoelomic metastasis of ovarian cancer. *J. Immunother. Cancer*. 9:e003973. <https://doi.org/10.1136/jitc-2021-003973>
- Ma, X. 2020. The omentum, a niche for premetastatic ovarian cancer. *J. Exp. Med.* 217:e20192312. <https://doi.org/10.1084/jem.20192312>
- Marillier, R.G., C. Uyttenhove, S. Goriely, E. Marbaix, and J. Van Snick. 2014. IL-27p28 is essential for parent-to-F1 acute graft-versus-host disease. *Eur. J. Immunol.* 44:2064–2073. <https://doi.org/10.1002/eji.201444491>
- Meza-Perez, S., and T.D. Randall. 2017. Immunological functions of the omentum. *Trends Immunol.* 38:526–536. <https://doi.org/10.1016/j.it.2017.03.002>
- Miller, C.H., S.G. Maher, and H.A. Young. 2009. Clinical use of interferon-gamma. *Ann. N. Y. Acad. Sci.* 1182:69–79. <https://doi.org/10.1111/j.1749-6632.2009.05069.x>
- Miyamoto, T., B. Murphy, and N. Zhang. 2023. Intraperitoneal metastasis of ovarian cancer: New insights on resident macrophages in the peritoneal cavity. *Front. Immunol.* 14:1104694. <https://doi.org/10.3389/fimmu.2023.1104694>
- Monk, B.J., N. Colombo, A.M. Oza, K. Fujiwara, M.J. Birrer, L. Randall, E.V. Poddubskaya, G. Scambia, Y.V. Shparyk, M.C. Lim, et al. 2021. Chemotherapy with or without avelumab followed by avelumab maintenance versus chemotherapy alone in patients with previously untreated epithelial ovarian cancer (JAVELIN ovarian 100): An open-label, randomised, phase 3 trial. *Lancet Oncol.* 22:1275–1289. [https://doi.org/10.1016/S1470-2045\(21\)00342-9](https://doi.org/10.1016/S1470-2045(21)00342-9)
- Nani, S., L. Fumagalli, U. Sinha, L. Kamen, P. Scapini, and G. Berton. 2015. Src family kinases and Syk are required for neutrophil extracellular trap formation in response to β -glucan particles. *J. Innate Immun.* 7:59–73. <https://doi.org/10.1159/000365249>
- Negoro, P.E., S. Xu, Z. Dagher, A. Hopke, J.L. Reedy, M.B. Feldman, N.S. Khan, A.L. Viens, N.J. Alexander, N.J. Attallah, et al. 2020. Splen tyrosine kinase is a critical regulator of neutrophil responses to *Candida* species. *mBio*. 11:e02043-19. <https://doi.org/10.1128/mBio.02043-19>
- Netea, M.G., L.A. Joosten, E. Latz, K.H. Mills, G. Natoli, H.G. Stunnenberg, L.A. O'Neill, and R.J. Xavier. 2016. Trained immunity: A program of innate immune memory in health and disease. *Science*. 352:aaf1098. <https://doi.org/10.1126/science.aaf1098>
- Netea, M.G., J. Quintin, and J.W. van der Meer. 2011. Trained immunity: A memory for innate host defense. *Cell Host Microbe*. 9:355–361. <https://doi.org/10.1016/j.chom.2011.04.006>
- Noy, R., and J.W. Pollard. 2014. Tumor-associated macrophages: From mechanisms to therapy. *Immunity*. 41:49–61. <https://doi.org/10.1016/j.immuni.2014.06.010>
- Patidar, A., S. Selvaraj, M. Chakravarti, I. Guha, A. Bhuniya, S. Bera, S. Dhar, K. Roy, R. Baral, D. Chattopadhyay, et al. 2022. TLR induced IL-27 plays host-protective role against B16BL6 melanoma in C57BL/6 mice. *Cytokine*. 154:155871. <https://doi.org/10.1016/j.cyt.2022.155871>
- Pflanz, S., J.C. Timans, J. Cheung, R. Rosales, H. Kanzler, J. Gilbert, L. Hibbert, T. Churakova, M. Travis, E. Vaisberg, et al. 2002. IL-27, a heterodimeric cytokine composed of EB13 and p28 protein, induces proliferation of naive CD4+ T cells. *Immunity*. 16:779–790. [https://doi.org/10.1016/S1074-7613\(02\)00324-2](https://doi.org/10.1016/S1074-7613(02)00324-2)
- Prat, J. 2014. Staging classification for cancer of the ovary, fallopian tube, and peritoneum. *Int. J. Gynaecol. Obstet.* 124:1–5. <https://doi.org/10.1016/j.ijgo.2013.10.001>
- Priem, B., M.M.T. van Leent, A.J.P. Teunissen, A.M. Sofias, V.P. Mourits, L. Willemsen, E.D. Klein, R.S. Oosterwijk, A.E. Meerwaldt, J. Munitz, et al. 2020. Trained immunity-promoting nanobiologic therapy suppresses tumor growth and potentiates checkpoint inhibition. *Cell*. 183:786–801.e19. <https://doi.org/10.1016/j.cell.2020.09.059>
- Pujade-Lauraine, E., K. Fujiwara, J.A. Ledermann, A.M. Oza, R. Kristeleit, I.L. Ray-Coquard, G.E. Richardson, C. Sessa, K. Yonemori, S. Banerjee, et al. 2021. Avelumab alone or in combination with chemotherapy versus chemotherapy alone in platinum-resistant or platinum-refractory ovarian cancer (JAVELIN ovarian 200): An open-label, three-arm, randomised, phase 3 study. *Lancet Oncol.* 22:1034–1046. [https://doi.org/10.1016/S1470-2045\(21\)00216-3](https://doi.org/10.1016/S1470-2045(21)00216-3)
- Quintin, J., S. Saeed, J.H.A. Martens, E.J. Giamarellos-Bourboulis, D.C. Ifrim, C. Logie, L. Jacobs, T. Jansen, B.J. Kullberg, C. Wijmenga, et al. 2012. *Candida albicans* infection affords protection against reinfection via

- functional reprogramming of monocytes. *Cell Host Microbe*. 12:223–232. <https://doi.org/10.1016/j.chom.2012.06.006>
- Raghavan, S., P. Mehta, Y. Xie, Y.L. Lei, and G. Mehta. 2019. Ovarian cancer stem cells and macrophages reciprocally interact through the WNT pathway to promote pro-tumoral and malignant phenotypes in 3D engineered microenvironments. *J. Immunother. Cancer*. 7:190. <https://doi.org/10.1186/s40425-019-0666-1>
- Rickard, B.P., C. Conrad, A.J. Sorrin, M.K. Ruhi, J.C. Reader, S.A. Huang, W. Franco, G. Scarcelli, W.J. Polacheck, D.M. Roque, et al. 2021. Malignant ascites in ovarian cancer: Cellular, acellular, and biophysical determinants of molecular characteristics and therapy response. *Cancers*. 13: 4318. <https://doi.org/10.3390/cancers13174318>
- Roby, K.F., C.C. Taylor, J.P. Sweetwood, Y. Cheng, J.L. Pace, O. Tawfik, D.L. Persons, P.G. Smith, and P.F. Terranova. 2000. Development of a syngeneic mouse model for events related to ovarian cancer. *Carcinogenesis*. 21:585–591. <https://doi.org/10.1093/carcin/21.4.585>
- Schreiber, R.D., A. Altman, and D.H. Katz. 1982. Identification of a T cell hybridoma that produces large quantities of macrophage-activating factor. *J. Exp. Med.* 156:677–689. <https://doi.org/10.1084/jem.156.3.677>
- Shepherd, T.G., and F.A. Dick. 2022. Principles of dormancy evident in high-grade serous ovarian cancer. *Cell Div.* 17:2. <https://doi.org/10.1186/s13008-022-00079-y>
- Shield, K., M.L. Ackland, N. Ahmed, and G.E. Rice. 2009. Multicellular spheroids in ovarian cancer metastases: Biology and pathology. *Gynecol. Oncol.* 113:143–148. <https://doi.org/10.1016/j.ygyno.2008.11.032>
- Siegel, R.L., K.D. Miller, N.S. Wagle, and A. Jemal. 2023. Cancer statistics, 2023. *CA Cancer J. Clin.* 73:17–48. <https://doi.org/10.3322/caac.21763>
- Smith, P., T. Bradley, L.M. Gavarró, T. Goranova, D.P. Ennis, H.B. Mirza, D. De Silva, A.M. Piskorz, C.M. Sauer, S. Al-Khalidi, et al. 2023. The copy number and mutational landscape of recurrent ovarian high-grade serous carcinoma. *Nat. Commun.* 14:4387. <https://doi.org/10.1038/s41467-023-39867-7>
- Street, K., D. Risso, R.B. Fletcher, D. Das, J. Ngai, N. Yosef, E. Purdom, and S. Dudoit. 2018. Slingshot: Cell lineage and pseudotime inference for single-cell transcriptomics. *BMC Genomics*. 19:477. <https://doi.org/10.1186/s12864-018-4772-0>
- Sun, L., T. Kees, A.S. Almeida, B. Liu, X.Y. He, D. Ng, X. Han, D.L. Spector, I.A. McNeish, P. Gimotty, et al. 2021. Activating a collaborative innate-adaptive immune response to control metastasis. *Cancer Cell*. 39: 1361–1374.e9. <https://doi.org/10.1016/j.ccell.2021.08.005>
- Svedersky, L.P., C.V. Benton, W.H. Berger, E. Rinderknecht, R.N. Harkins, and M.A. Palladino. 1984. Biological and antigenic similarities of murine interferon-gamma and macrophage-activating factor. *J. Exp. Med.* 159: 812–827. <https://doi.org/10.1084/jem.159.3.812>
- van Rooijen, N., and E. Hendriks. 2010. Liposomes for specific depletion of macrophages from organs and tissues. *Methods Mol. Biol.* 605:189–203. https://doi.org/10.1007/978-1-60327-360-2_13
- Vázquez-García, I., F. Uhlitz, N. Ceglia, J.L.P. Lim, M. Wu, N. Mohibullah, J. Niyazov, A.E.B. Ruiz, K.M. Boehm, V. Bojilova, et al. 2022. Ovarian cancer mutational processes drive site-specific immune evasion. *Nature*. 612:778–786. <https://doi.org/10.1038/s41586-022-05496-1>
- Vega-Pérez, A., L.H. Villarrubia, C. Godio, A. Gutiérrez-González, L. Feo-Lucas, M. Ferriz, N. Martínez-Puente, J. Alcaín, A. Mora, G. Sabio, et al. 2021. Resident macrophage-dependent immune cell scaffolds drive anti-bacterial defense in the peritoneal cavity. *Immunity*. 54:2578–2594.e5. <https://doi.org/10.1016/j.immuni.2021.10.007>
- Walton, J., J. Blagih, D. Ennis, E. Leung, S. Dowson, M. Farquharson, L.A. Tookman, C. Orange, D. Athineos, S. Mason, et al. 2016. CRISPR/Cas9-Mediated Trp53 and Brca2 knockout to generate improved murine models of ovarian high-grade serous carcinoma. *Cancer Res.* 76: 6118–6129. <https://doi.org/10.1158/0008-5472.CAN-16-1272>
- Ward Rashidi, M.R., P. Mehta, M. Bregenzner, S. Raghavan, E.M. Fleck, E.N. Horst, Z. Harissa, V. Ravikumar, S. Brady, A. Bild, et al. 2019. Engineered 3D model of cancer stem cell enrichment and chemoresistance. *Neoplasia*. 21:822–836. <https://doi.org/10.1016/j.neo.2019.06.005>
- Wattenberg, M.M., H. Coho, V.M. Herrera, K. Graham, M.L. Stone, Y. Xue, R.B. Chang, C. Cassella, M. Liu, S. Choi-Bose, et al. 2023. Cancer immunotherapy via synergistic coactivation of myeloid receptors CD40 and Dectin-1. *Sci. Immunol.* 8:eadj5097. <https://doi.org/10.1126/sciimmunol.adj5097>
- Wiemann, B., and C.O. Starnes. 1994. Coley's toxins, tumor necrosis factor and cancer research: A historical perspective. *Pharmacol. Ther.* 64: 529–564. [https://doi.org/10.1016/0163-7258\(94\)90023-X](https://doi.org/10.1016/0163-7258(94)90023-X)
- Woeste, M.R., R. Shrestha, A.E. Geller, S. Li, D. Montoya-Durango, C. Ding, X. Hu, H. Li, A. Puckett, R.A. Mitchell, et al. 2023. Irreversible electroporation augments β -glucan induced trained innate immunity for the treatment of pancreatic ductal adenocarcinoma. *J. Immunother. Cancer*. 11:e006221. <https://doi.org/10.1136/jitc-2022-006221>
- Xia, H., S. Li, X. Li, W. Wang, Y. Bian, S. Wei, S. Grove, W. Wang, L. Vatan, J.R. Liu, et al. 2020. Autophagic adaptation to oxidative stress alters peritoneal residential macrophage survival and ovarian cancer metastasis. *JCI Insight*. 5:e141115. <https://doi.org/10.1172/jci.insight.141115>
- Yang, H., L. Xia, J. Chen, S. Zhang, V. Martin, Q. Li, S. Lin, J. Chen, J. Calmette, M. Lu, et al. 2019. Stress-glucocorticoid-TSC2D3 axis compromises therapy-induced antitumor immunity. *Nat. Med.* 25:1428–1441. <https://doi.org/10.1038/s41591-019-0566-4>
- Yoshida, H., and C.A. Hunter. 2015. The immunobiology of interleukin-27. *Annu. Rev. Immunol.* 33:417–443. <https://doi.org/10.1146/annurev-immunol-032414-112134>
- Zhang, N., R.S. Czepielewski, N.N. Jarjour, E.C. Erlich, E. Esaulova, B.T. Saunders, S.P. Grover, A.C. Cleuren, G.J. Broze, B.T. Edelson, et al. 2019. Expression of factor V by resident macrophages boosts host defense in the peritoneal cavity. *J. Exp. Med.* 216:1291–1300. <https://doi.org/10.1084/jem.20182024>
- Zhang, N., S.H. Kim, A. Gainullina, E.C. Erlich, E.J. Onufer, J. Kim, R.S. Czepielewski, B.A. Helmink, J.R. Dominguez, B.T. Saunders, et al. 2021a. LYVE1+ macrophages of murine peritoneal mesothelium promote omentum-independent ovarian tumor growth. *J. Exp. Med.* 218: e20210924. <https://doi.org/10.1084/jem.20210924>
- Zhang, S., S. Iyer, H. Ran, I. Dolgalev, S. Gu, W. Wei, C.J.R. Foster, C.A. Loomis, N. Olvera, F. Dao, et al. 2021b. Genetically defined, syngeneic organoid platform for developing combination therapies for ovarian cancer. *Cancer Discov.* 11:362–383. <https://doi.org/10.1158/2159-8290.CD-20-0455>
- Zhu, F., D. Jing, H. Zhou, Z. Hu, Y. Wang, G. Jin, Y. Yang, and G. Zhou. 2023. Blockade of Syk modulates neutrophil immune-responses via the mTOR/RUBCNL-dependent autophagy pathway to alleviate intestinal inflammation in ulcerative colitis. *Precis. Clin. Med.* 6:pbad025. <https://doi.org/10.1093/pcmedi/pbad025>

Supplemental material

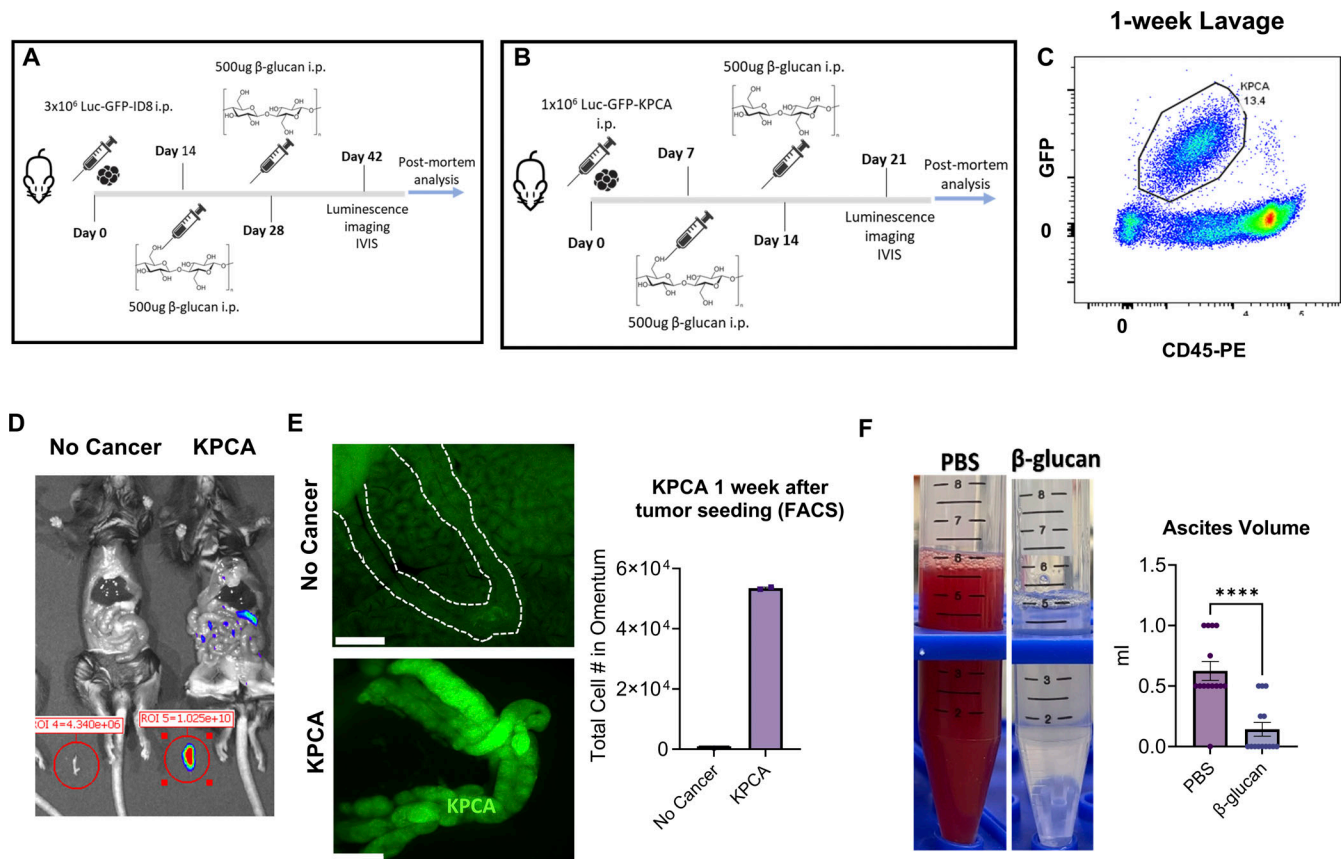


Figure S1. **KPCA tumors model stage III OvCa and β -glucan treatment clears ascites.** (A and B) Treatment timelines of (A) ID8 and (B) KPCA tumors treated with β -glucan. (C) Representative flow plot identifying GFP+CD45⁻ KPCA cells in the peritoneal lavage of mice 1 wk after tumor seeding. (D) Representative image and quantification of compartmental bioluminescent imaging. The omentum is removed from the cavity; signals (red circle) are obtained separately from the rest of the peritoneal cavity (non-omentum signal). (E) Representative fluorescent images of the omentum and KPCA numbers in the omentum of mice 1 wk after KPCA cell injection. Scale bar is 2.5 mm. (F) Representative images of ascites and calculated changes in ascites volumes from PBS- or β -glucan-treated mice. Student's *t* test was used. *****P* < 0.0001. Error bars are standard errors of the mean.

Downloaded from http://rupress.org/jem/article-pdf/221/12/e20231967/1935301/jem_20231967.pdf by Univ Of Penn Library user on 11 March 2025

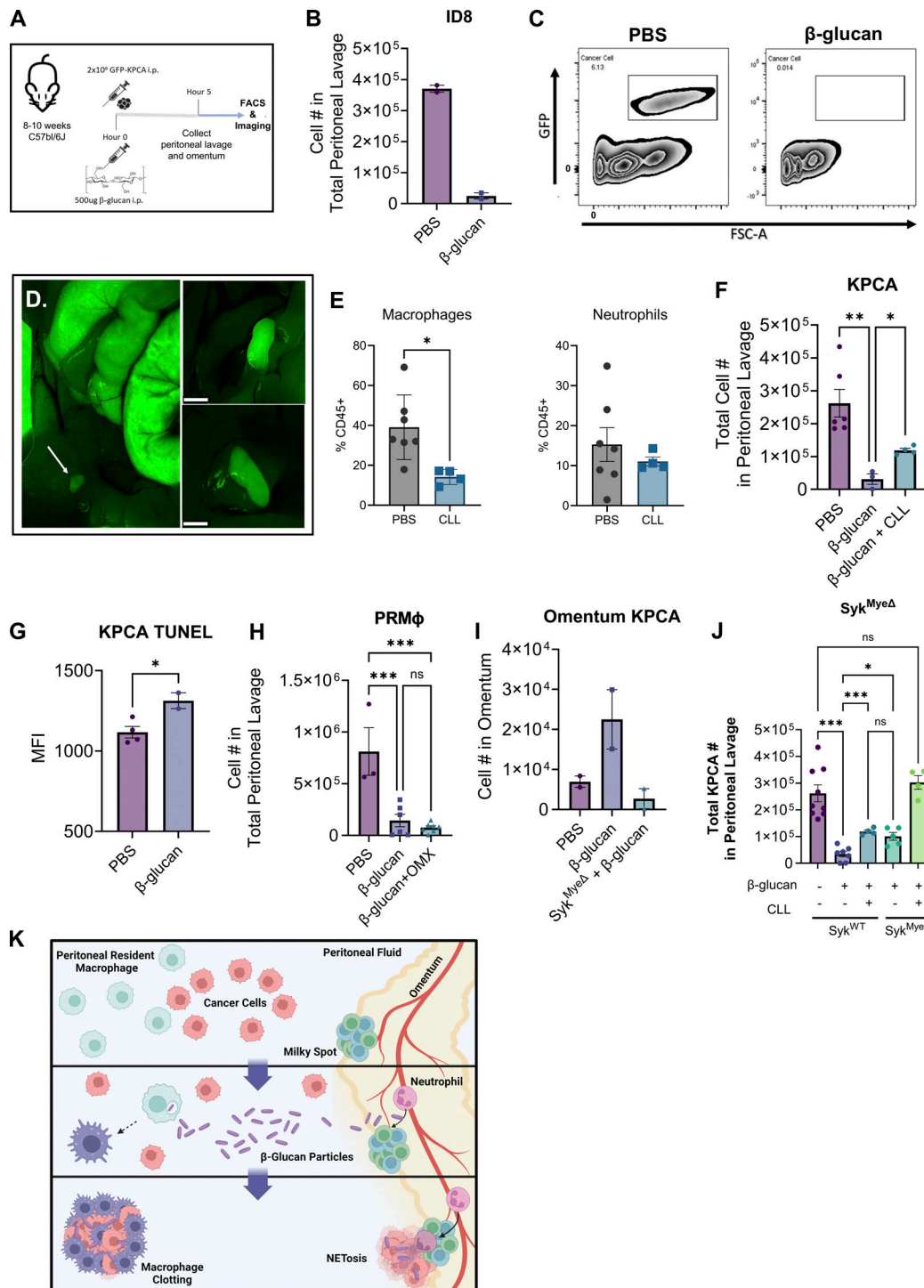


Figure S2. β-glucan captures OvCa cells into solid nodular structures via intraperitoneal clotting and Dectin-1-Syk-dependent NETosis in the omentum. (A) Acute cancer cell capture timeline. (B) Quantification of ID8 cells in the peritoneal lavage of mice 5 h after β-glucan treatment. (C) Representative flow plots of GFP+ KPCA cells disappearing from the peritoneal lavage 5 h after intraperitoneal β-glucan administration. (D) Representative in situ images of peritoneal clots formed in the peritoneal cavity after β-glucan treatment. These clots contain GFP+ KPCA cancer cells. Scale bars are 1 mm. (E) Quantification of macrophages and neutrophils in the peritoneal fluid following CLL administration as analyzed by flow cytometry. (F) Quantification of KPCA cells in peritoneal lavage as determined by flow cytometry in control or CLL-pretreated mice 5 h after intraperitoneal β-glucan administration. (G) MFI of TUNEL staining in KPCA cells in the clots β-glucan-treated mice and peritoneal lavage from PBS-treated mice, which do not form clots. (H) Quantification of PRMΦs in the peritoneal lavage of control or OMX mice after β-glucan administration. (I) Quantification by flow of GFP+ KPCA cells in the omentum of Syk^{WT} and Syk^{MyeΔ} mice treated with β-glucan. (J) Quantification of KPCA cells in peritoneal lavage in Syk^{WT} and Syk^{MyeΔ} mice 5 h after indicated treatment with PBS, β-glucan, or CLL. (K) Graphical representation of two mechanisms of cancer cell capture following intraperitoneal injection of β-glucan. Illustration created with <https://biorender.com>. Graphs are represented by combined data of three or more independent runs. One-way ANOVA and Student's *t* test were used. **P* < 0.05; ***P* < 0.01; ****P* < 0.001. Error bars are standard errors of the mean.

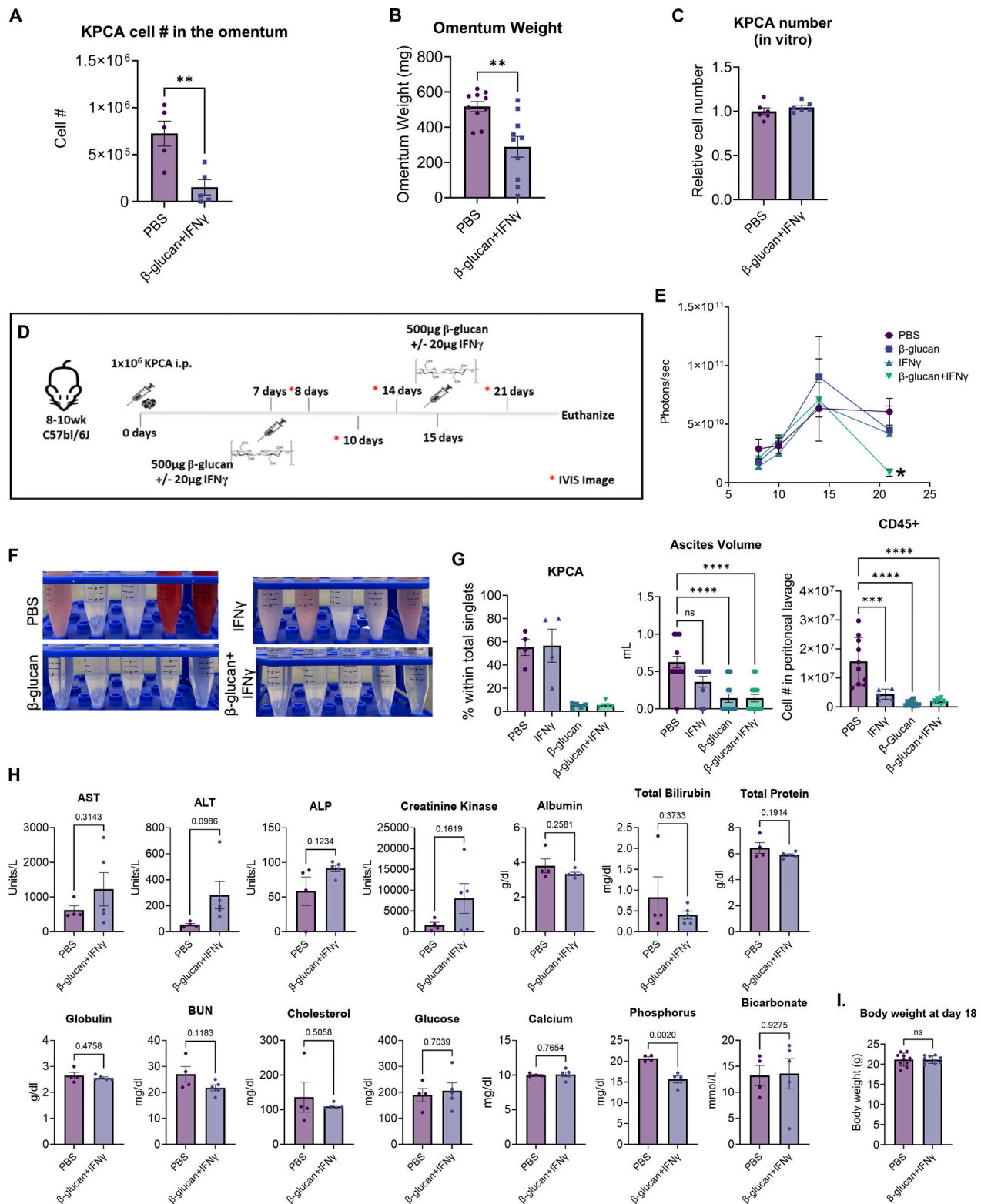


Figure S3. **Analyses of tumor burden and toxicity after BI treatments.** (A and B) (A) KPCA cell numbers in the omentum evaluated by flow cytometry and (B) omentum tumor weight in PBS- or BI-treated mice. (C) Quantification of KPCA numbers 48 h following PBS and BI treatment in vitro. Student's *t* test was used. (D) Treatment and longitudinal imaging timeline in PBS-, IFN γ -, β -glucan-, and BI-treated mice. (E) Quantification of bioluminescence signals in mice tracked longitudinally from day 8 to day 21 after tumor seeding. (F and G) (F) Representative images of ascites accumulation and (G) quantification of KPCA cells and CD45+ cells and ascites volumes based on the peritoneal lavage of mice treated with PBS, IFN γ , β -glucan, and BI 21 days after tumor seeding. (H) IDEXX clinical chemistry analyses of sera from PBS- or BI-treated mice. (I) Body weight of PBS- or BI-treated mice 18 days after tumor cell seeding. Graphs are represented by combined data of three or more independent runs. Student's *t* test and one-way ANOVA were used **P* < 0.05, ***P* < 0.01, ****P* < 0.001, *****P* < 0.0001. Error bars are standard errors of the mean.

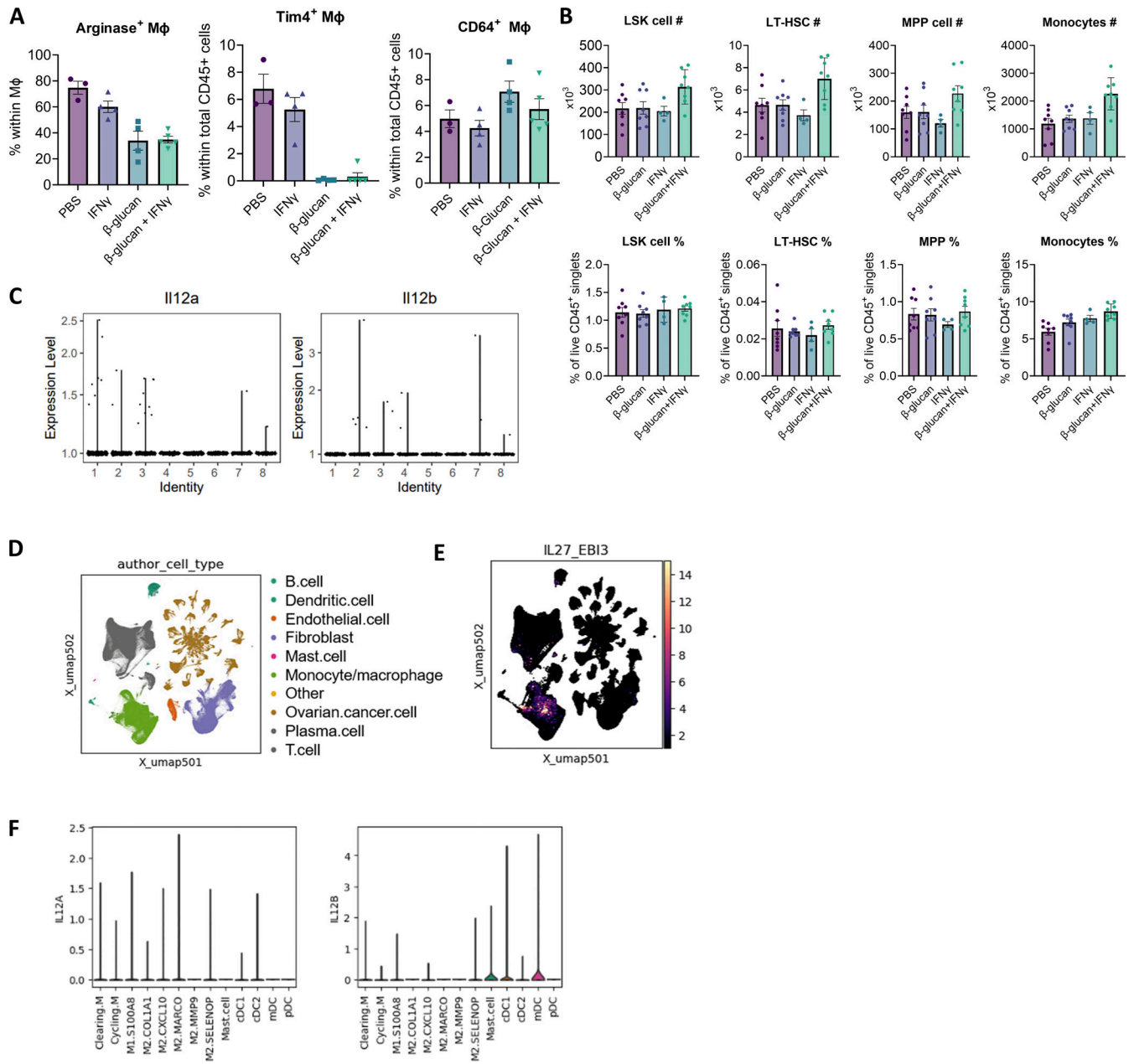


Figure S4. Impact BI on MΦs, monocytes and myeloid progenitor cells and scRNA-seq of mouse and patient datasets. (A) Quantification of frequencies of Arginase⁺ MΦs, Tim4⁺ MΦs, and CD64⁺ MΦs in omentum tumors treated as indicated and determined by flow cytometry. **(B)** Number of progenitor cells and monocytes in the bone marrow of mice 1 wk after PBS or BI treatment. LSK, Lin-Sca1+cKit⁺ progenitor cells; LT-HSC, long-term hematopoietic stem cells; MPP, multipotent progenitor cells. **(C)** Expression of *IL12a* and *IL12b* in monocyte/MΦ clusters pooled from mice treated with PBS, β-glucan, IFNγ, or BI. **(D and E)** (D) Uniform manifold approximation and projection (UMAP) plot of immune cells and (E) co-expression of *IL27-EBI3* in human OvCa patient tumors. **(F)** Expression of *IL12A* and *IL12B* in each myeloid cell subcluster from human OvCa tumors. Graphs are represented by combined data of three or more independent runs. Student's *t* test was used. **P* < 0.05. Error bars are standard errors of the mean.

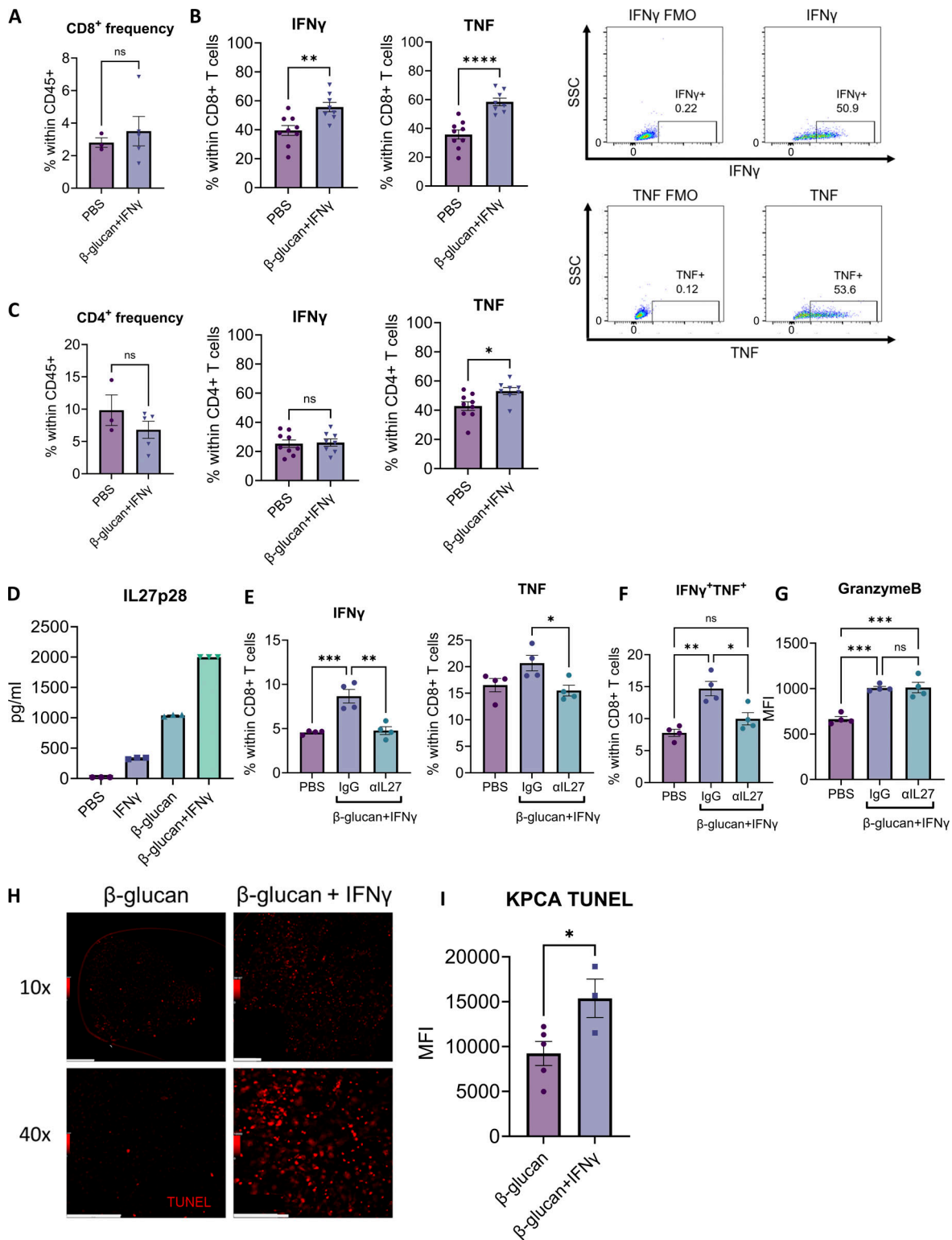


Figure S5. BI activates T cells in an IL27-dependent manner and kills KPCA cells. (A and B) (A) Quantification of frequencies and (B) activation of CD8⁺ T cells in omentum tumors from PBS- or BI-treated mice and flow cytometry plots of TNF- or IFN γ -stained samples, including fluorescence minus one (FMO) plots used to identify positive populations. (C) Quantification of frequencies and activation of CD4⁺ T cells in omentum tumors from PBS- or BI-treated mice. (D) ELISA quantification of IL30 (IL27p28) in supernatant from BMDM cultured with PBS, IFN γ , β -glucan, and BI. (E-G) Frequencies of (E) IFN γ ⁺ or TNF⁺, (F) IFN γ ⁺TNF⁺ CD8⁺ T cells, and (G) Granzyme B MFI of CD8⁺ T cells cocultured with M Φ pretreated with PBS or BI in the presence of α IL27 antibody or control IgG. (H) Representative TUNEL staining in β -glucan- or BI-induced clots. Scale bars are 500 μ m. (I) FACS quantification TUNEL MFI in GFP+ KPCA cells. In vivo data combined from three independent runs plotted where each dot represents one mouse. One representative run presented for in vitro data where each dot represents one replicate. Student's *t* test and one-way ANOVA were used. **P* < 0.05; ***P* < 0.01; ****P* < 0.001; *****P* < 0.0001. Error bars are standard errors of the mean.

Provided online is Table S1, which lists information for all antibodies used in this study.